Biointerface Research in Applied Chemistry
Open-Access Journal (ISSN: 2069-5837)

Article
Volume 13, Issue 5, 2023, 435
https://doi.org/10.33263/BRIAC135.435

Thermodynamics and Conformational Dynamics of Primer Nucleotide Sequences Associated with Monkeypox Virus (MpxV): Comparative Analysis of Stability and Specificity with a Biophysical-Computational Approach

Lenin González-Paz [1,*], Carla Lossada [1], María Laura Hurtado-León [2], Joan Vera-Villalobos [3], José Luis Paz [4], David S. Coll [5], Laura N. Jeffreys [6], Yovani Marrero-Ponce [7], Ysaias J. Alvarado [8,*]

1 Venezuelan Institute of Scientific Research. Molecular Biomedicine Center, Biocomputing Laboratory. Maracaibo, Zulia, Bolivarian Republic of Venezuela; lgonzalezpaz@gmail.com (L.G.P); lossadacarla@gmail.com (C.L.);
2 University of Zulia. Experimental Faculty of Sciences. Biology department. Maracaibo – Zulia, Bolivarian Republic of Venezuela; marialahurtado@gmail.com (M.L.H.L);
3 Faculty of Natural Sciences and Mathematics, Department of Chemistry and Environmental Sciences, Instrumental Chemical Analysis Laboratory, Escuela Superior Politécnica del Litoral, Guayaquil, Ecuador; joarvera@espol.edu.ec (J.V.V.);
4 Academic Department of Inorganic Chemistry, Faculty of Chemistry and Chemical Engineering, Universidad Nacional Mayor de San Marcos. Lima Peru; jpazr@unmsm.edu.pe (J.L.P.);
5 Venezuelan Institute of Scientific Research. Chemistry Center. Laboratory of Theoretical Physicochemistry of Materials; dsantiag@ivic.gob.ve (D.S.C.);
6 Centre for Drugs and Diagnostics, Department of Tropical Disease Biology, Liverpool School of Tropical Medicine, Pembroke Place, Liverpool L3 5QA, UK; laura.jeffreys@lstmed.ac.uk (L.N.J.);
7 San Francisco de Quito University, Molecular and Translational Medicine Group, College of Health Sciences, School of Medicine, Medical Specialties Building; and Institute of Computational Simulation, Diego de Robles y vía Interoceánica, Quito, 170157, Pichincha, Ecuador; ymarrero@usfq.edu.ec (Y.M.P.);
8 Venezuelan Institute of Scientific Research. Center for Molecular Biomedicine, Laboratory of Theoretical and Experimental Biophysical Chemistry. Maracaibo, Zulia, Bolivarian Republic of Venezuela; alvaradoysaias@gmail.com (Y.J.A.);
* Correspondence: lgonzalezpaz@gmail.com (L.G.P); alvaradoysaias@gmail.com (Y.J.A.);
Scopus Author ID 6602882448; 57222578554

Received: 7.09.2022; Accepted: 7.10.2022; Published: 19.12.2022

Abstract: COVID-19 pandemic has shown the need to detect new pathogens quickly. Currently, attention has been paid to the recent epidemic of the Monkeypox virus (MpxV), the etiological agent of the zoonotic disease monkeypox. As happened with COVID-19, diagnosis is the priority in public health interventions. In MpxV infection, PCR is routinely used to detect the viruses. However, the utility of the method is dependent on designing PCR-efficient primers. Therefore, it is important to consider computational approaches that adopt various parameters, including thermodynamics, in order to offer increasingly efficient PCRs. We propose to determine the stability of primers for the specific detection of MpxV considering the thermodynamics of folding. For this, primers directed to specific genes were designed, classified, and reclassified. Furthermore, we propose to determine their theoretical aggregation in an aqueous model guided by molecular dynamics to offer optimal primers. A relationship was observed between the thermodynamic stability and the conformational fluctuations of the primers in an aqueous medium. The thermodynamic stability of the primers designed by standard methods could be discriminated by the prediction of DNA folding at a constant temperature. The variability observed in the primers after being reclassified shows an interaction between the thermodynamic stability and conformational fluctuations in solution, which could affect the efficiency of the PCR reactions. Therefore, under the conditions of this study, we propose to consider specific primers targeting the

OPG191 gene of MpxV for experimental demonstrations since they present additional optimal characteristics in terms of thermal stability and dynamic.

Keywords: orthopoxviruses; SWAXS curve; molecular dynamics; OPG; primers.

1. Introduction

Orthopoxviruses (ORPV) comprise a genus within the subfamily *Chordopoxvirinae* of the family *Poxviridae*. These viruses infect diverse mammalian hosts, including, in some cases, humans, typically through animal reservoirs. For example, smallpox (variola) virus (VarV) and *Monkeypox virus* (MpxV) [1]. Orthopox viruses (OPV) are characterized by their large brick shape and double-stranded DNA [2]. These viruses have been responsible for many large-scale epidemics caused by VarV. Indeed, it is estimated that smallpox caused the deaths of over 300 million people [3]. Despite having a highly effective vaccine, there are no effective treatments for smallpox. And so, a massive global vaccination effort was undertaken to eradicate the disease.

Recently, an outbreak of monkeypox has spread to 42 countries. MpxV is the etiological agent of the zoonotic disease monkeypox, which was first identified as a human pathogen in the Democratic Republic of the Congo (DRC). In the 50 years since human cases of MpxV have been identified in 11 African countries, and MpxV is considered endemic in the DRC [2]. Between 1970 and 1986, >400 monkeypox cases were reported in Africa. Of these cases, 95% were reported within the DRC [5]. Until the 2003 US outbreak, no human cases had been reported outside of Africa [6].

These events were followed by the largest MpxV outbreak in West Africa, in Nigeria, in 2017. Followed by the reporting in Singapore [4]. The resurgence of this virus was observed in 2022, with the report of cases of MpxV in Portugal, Spain, Canada, Belgium, Sweden, Italy, Australia, France, Germany, the Netherlands and the United Kingdom, Switzerland, Israel, and Denmark. On May 24, 2022, the Czech Republic confirmed its first case, as did the United Arab Emirates and Slovenia [7,8]. Recently, with the simultaneous pandemic of COVID-19, there is an ongoing outbreak between European and non-European countries, with almost 3,000 confirmed cases as of June 21, 2022 [9]. Further cases have been reported in Europe, North America, and other parts of the globe: https://www.cdc.gov/poxvirus/monkeypox/response/2022/world-map.html.

Mpx, typically presents with symptoms like discrete, ordinary smallpox. After about a 2-week, asymptomatic incubation period, infected individuals develop fever followed by a disseminated rash. Both illnesses are transmissible between humans and can result in death [10]. The case fatality rate for monkeypox is much lower than for smallpox, as is the rate of human-to-human transmissibility [6]. A multicomponent surveillance and containment strategy is recommended in the case of a smallpox outbreak. A critical component of this strategy is the early detection of a smallpox case. A detection delay is likely to impact the overall control strategy [6] considerably. Since MpxV has demonstrated its ability to exploit new hosts and move globally, several nucleic acid assay methods have been developed for its detection and characterization [6,11-14]. In fact, PCR blood tests are not conclusive in diagnosing human monkeypox because the virus remains in the blood only for a short time. Therefore, PCR tests of skin lesions (surface and/or exudate, roofs, or crusts) are the preferred diagnostic testing method for virus detection [15].

Similarly, as it happened for COVID-19, reliable laboratory diagnosis is among the main priorities to facilitate public health interventions. At present, there are a few primer sequence sets for PCR assays for OrpV (using EN ISO 15189) accredited diagnostic methods; for instance, a qPCR assay for simultaneous detection of all OrpV species (Real-Star *Orthopoxvirus* Kit, Altona Diagnostics, Germany) and specifically MpxV that can be used for the development and control of laboratory tests. For example, in MpxV infection, PCR (polymerase chain reaction) is routinely used to detect the viruses that cause the zoonotic disease monkeypox [6].

Routine detection of specific MpxV DNA from clinical/veterinary specimens is accomplished by (RT)-PCR targeting conserved regions of extracellular-envelope protein gene (B6R) [6], DNA polymerase gene, E9L [16,17], and DNA-dependent RNA polymerase subunit 18, rpo18 [18]. In addition, Li *et al*. noted that the C3L gene associated with the complement binding protein is recommended for PCR assays for the detection of MpxV from the Congo Basin [12]. More recently, alternatives have been developed for the simultaneous detection of both MpxV clades, such as recombinase polymerase amplification (RPA, an alternative method to (RT)-PCR), which was proposed for the detection of the gene associated with Tumor necrosis factor (TNF)-binding protein, which is present in inverted repeats of the MPXV genome [19]. In conclusion, PCR kits detecting specifically MpxV are under development [20,21], however, there are no commercial PCR or serology kits available, representing a global public health problem.

The feasibility of introducing robust PCR-based detection technology in public health laboratories during international health emergencies has been previously demonstrated [22]. PCR is fundamental to molecular biology and is the most important practical molecular technique for the DNA research laboratory. However, the method's utility depends on identifying unique primer sequences and designing PCR-efficient primers. Primer design is a critical step in all types of PCR methods to ensure specific and efficient target sequence amplification. Even though there are currently many online and commercial bioinformatics tools, primer design for PCR is still not as convenient and practical as it might be for routine use [23-26]. Therefore, it is important to consider various computational approaches that adopt various parameters, including thermodynamic approaches, in order to offer increasingly efficient PCRs in terms of optimal primer pair combinations [27]. Especially because the hybridization between the PCR primer and the DNA template is a thermodynamic reaction, thus, it is not sufficient to determine binding sites by merely using sequence alignment programs such as BLAST (Basic Local Alignment Search Tool) [28]. For example, the G–C and A–T matches have equal scores in an NCBI (National Center for Biotechnology Information)-BLAST search, but the G–C match is more stable than the A–T match [29]. Even a mismatch, such as G–G, contributes as much as ≈-2 kcal/mol (Gibbs free energy) to the duplex stability. Therefore, the thermodynamic approach should be applied to reasonably predict primer binding sites [30].

Primer design requires the calculation of various metrics to assess various aspects of primer quality and then combining these individual metrics and propose quality scores such as primer melt temperature, the thermodynamic stability of a primer at the 3′-end, and a variety of other criteria motivated by practical experience with PCR. However, selecting primers with ideal thermodynamic characteristics presents difficulties that must be considered. Firstly, the conventional metrics used cannot always adequately interpret the physical characteristics of molecules and secondly, they can become redundant. For example, one of the main

requirements when designing PCR primers is that they must not bind to other primers and generate dimers. These calculations are considered in popular tools like Primer3 [31,32] uses twoSmith–Waterman alignment-based metrics to assess the likelihood of a primer binding to itself or the other primer: the max-complementarity metric and the max-3′-complementarity. The main difference between these metrics is that the first considers the total similarity between a pair of sequences or primers, and the second considers the localized similarity at the 3′ ends. However, these metrics tend to be redundant because high 3′ local similarities are also associated with high total similarity, making them thermodynamically incorrect predictions because they do not consider the effects described in DNA-binding interactions [29].

In this sense, we propose to determine the thermodynamic stability of primers for the specific detection of MpxV by *in silico* amplification of 8 genes of interest (see in the next section), both at the level of the formation of dimers and hairpins and at the level of thermodynamic stability in DNA binding. Also, in order to offer optimal potential primers designed with a biophysical-computational approach, we propose to determine their theoretical aggregation in an aqueous model guided by molecular dynamics. It is important to point out that this study does not intend to indicate which target is the most suitable for the design of primers directed at MpxV, nor does it seek to invalidate any of the primers designed with the proposed tools.

This study seeks to propose an alternative strategy to characterize and discriminate between primers considering parameters of molecular folding and its dynamics to optimize PCR *in silico* reactions at a thermodynamic level from a biophysical-computational point of view. In addition, we show that the approach proposed here can reproduce the thermodynamic stability of the molecular folding of the published primers for detecting MpxV by PCR.

2. Materials and Methods

2.1. Genes of interest associated with Monkeypox virus (MpxV).

Genetic sequences widely distributed and reported as being of interest in the MpxV were used for the design of the primers, specifically the E5R gene (OPG117), which has been recommended because it is a sequence similar to that of the *Vaccinia Copenhagen* D5R strain, and is associated to a nucleic acid-independent nucleoside triphosphatase [1, 4, 33]; E6R gene (OPG118) which is similar in sequence to that of the *Vaccinia Copenhagen* strain D6R and is associated with an early transcription factor, VETF [1,4,34]; C3L gene (OPG032), suggested to be similar to the complement control protein (CCP), and to participate in the prevention of complement activation [1,4]; N1L gene (OPG035) recommended for being associated with the Bcl-2 domain and inhibition of NF-kB-mediated activation and apoptosis [1,4]; F3L gene (OPG047) which is associated with the BTB and Kelch domains, and contributes to virulence [1,4]; B6R gene (OPG190) associated with HEAT/ARM-like repeats and with the C-terminal transmembrane domain [1,4]; B7R gene (OPG191) associated with the PIE domain "*Poxvirus* Immune Evasion" and contribution to virulence, resident of ER and SCP-3; and the B15R gene (OPG200) associated with the Bcl-2 domain, inhibition of NF-kB signaling, prevention of IkBα phosphorylation and regulation of MAPK/AP-1 activation [1,4]. All genes of interest were obtained from NCBI/GenBank (https://www.ncbi.nlm.nih.gov/).

Figure 1 shows the pipeline used in this report for primer design and quality control. First, we used NCBI's primer specificity analysis and design software, Primer3-BLAST [32,35], to screen several candidate primer pairs. Second, for each pair of candidate primers,

we used MFEprimer [22] to analyze their specificity, dimers, and hairpins, followed by FastPCR [25,36,37] to calculate reaction efficiencies and DNAFold [38,39] for the prediction of thermodynamic fold stability, as well as a series of molecular dynamics tools to complement stability calculations. These phases are detailed in the following sections:

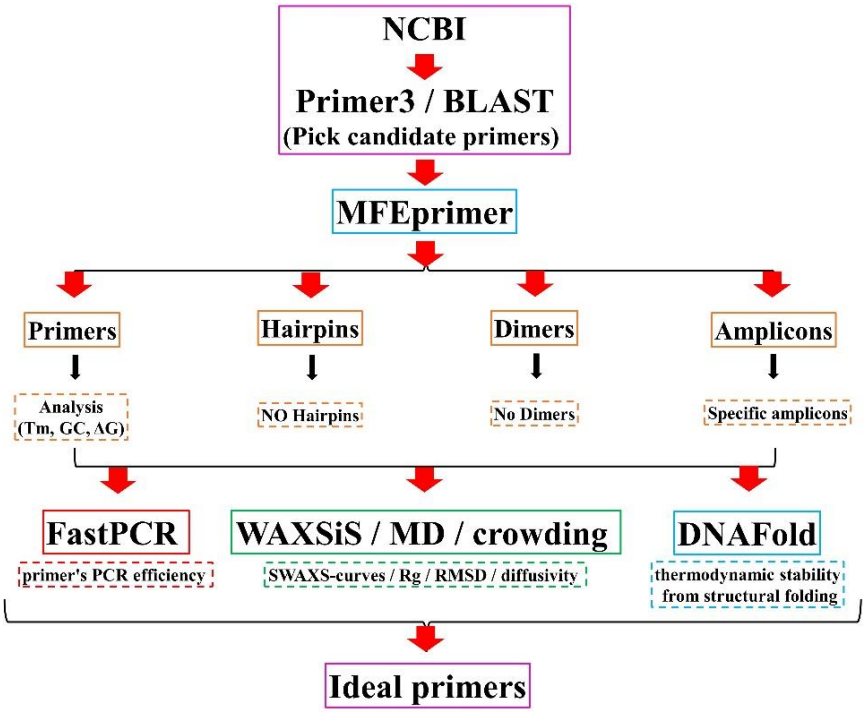

Figure 1. The pipeline used for the design and quality control of primers directed to genes associated with MpxV.

2.2. Design of primers for MpxV.

A standard design of specific primers was performed using the NCBI/GenBank Primer3 and BLAST algorithms (https://www.ncbi.nlm.nih.gov/tools/primer-blast/) [32,35]. This strategy allows screening for nonspecific binding sites prior to primer design using species-specific mispriming libraries or integrated genome-wide nonspecific binding site search with the entire genome as a template. Specifically, potential oligonucleotide primers were designed with the Primer3 program [32,35] and tested for the absence of homology to the nucleotide sequences of other representative viruses and genomes, including the human with the help of the BLAST program [28]. The criteria for selecting the primers were the specific amplification of the DNA associated with the genes of interest of the ORPV MpxV species regardless of the presence of other poxvirus DNA and that the length of the amplicon produced does not exceed 500 bp. Initially, 30 primer pairs were selected for each gene of interest (Table S1).

2.3. Quality control of the specificity and thermodynamic stability of primers.

Once the primers were designed, a two-phase quality control (QC) was performed: 1) characterization and classification of the primers following the criteria of specificity and stability of sequences with the "prior-to" strategy applying the *k-mer* algorithm, followed by a validation analysis of thermodynamic stability and PCR *in silico* with the FastPCR software [25,36,37], and 2) a reclassification by analyzing the energetic contributions of the primer sequences of interest to the PCR reaction, studying the thermodynamic stability of the folding of primers at a constant temperature. This was done because although primer design strategies

share similar primer quality control parameters, such as the prevention of unwanted amplicons, dimers, and hairpins, few apply a search process using a *k-mer*-based algorithm. This "prior-to" strategy is important to reduce the probability of primers binding to repeated regions. In this sense, the MFEprimer tool (https://mfeprimer3.igenetech.com/) [22], a functional and independent primer quality control program, was considered. Which features improved sensitivity with which specificity can be assessed using an updated *k-mer* algorithm, which allows discrepancies within the *k-mer* except for the first base at the 3′ end; it is also an algorithm that allows quick identification of autodimers, crossed dimers, and hairpins; allows to verify the SNPs (Single Nucleotide Polymorphism) of the binding sites, which will affect the binding efficiency in the PCR reactions [22]. The selected primers were compared with the NCBI virus database represented by 143747 complete genomes, updated as of 2020-07-04, and against the *Homo sapiens* (human) genome of the Genome Reference Consortium Human Build 37 (GRCh37) updated as of 2009-02-27, provided by the MFEprimer-3.1 server (https://mfeprimer3.igenetech.com/). In addition, the primers were compared to the *Homo sapiens* (human) sequence from the Genome Reference Consortium, Human Build 38 patch release 14 (GRCh38.p14) (https://www.ncbi.nlm.nih.gov/assembly/GCF_000001405.40) (Date: 2022-02-03).

Additionally, FastPCR software (http://primerdigital.com/) [25,36,37] was used, which is an environment of integrated tools for designing PCR primers and probes and for predicting oligonucleotide properties. The software provides comprehensive tools to design primers for most PCR applications. *In silico* PCR primers or probes, the search includes comprehensive analyses of single primers and primer pairs. This strategy provides an integrated analysis of the sequences and allows the calculation of characteristics or physical properties of the nucleotide sequence, such as length, CG content, and melting temperature. Melting temperature predictions use thermodynamic parameters as the nearest neighbor for standard and degenerate oligonucleotides, including locked nucleic acids (LNAs) and other modifications, and provide a dilution and resuspension calculator for stocks [13,27].

In order to increase the rigor of the comparative analysis, the prediction of DNA folding was used with the DNAfold module (of the Mfold server) [38,39], which has specific parameters for DNA analysis that include stacking, mismatches and hanging ends, which were proposed and measured experimentally by the Santa Lucia group (John SantaLuica Jr., Department of Chemistry, Wayne State University, Detroit, MI). The DNAfold module (http://www.unafold.org/mfold/applications/dna-folding-form.php) of the Mfold server comprises a tool that predicts the folding, hybridization, and melting temperatures of nucleotides. As with the free energy parameters, the enthalpies are measured at 37 °C. The stability of the primers was studied at 37 °C due to several reasons; first, it has been shown that DNA degradation is greatly affected by room temperature and may even be lost by aggregation [40]. On the other hand, the predictions of free energy and enthalpy contributions (from the DNA folding algorithm) have been standardized using experimental data at 37 °C [41]. In addition, it has been described that these parameters tend to be constant within the temperature range that can occur in vivo or in vitro [41]. Additionally, the DNA folding stability model used considers experimental data based on the approach of nearest-neighbor stabilities at 37 °C for predictions [40,41]. Primer melting is generally carried out in solutions with low salt concentration. The thermodynamic results are extrapolated to the standard state temperature of 37 °C, since the thermal denaturation data of polymers are difficult to obtain and interpret correctly because their transitions are not usually two-state (i.e., many developmental

intermediates are possible). Their melting temperatures are high [40-43]. This tool for calculating thermodynamic stability from structural folding is accurate, showing failure rates of <1% [41].

2.4. Molecular dynamics (MD) of primers.

MD simulations were performed with YASARA Dynamics software [44]. YASARA allows you to perform MD simulations automatically from structures in PDB format. YASARA adds both the missing hydrogens and heavy atoms, fixing steric clash issues and solving other common problems in unprepared PDB files. First, the primer PDB file was loaded into a cuboid simulation box with water and explicit counter ions. Next, nucleotide atoms were determined by the AMBER03 force field offered by YASARA [45], and the TIP3P water model was adopted [46]. In YASARA, the backbone atoms and heavy atoms have restricted positions (with force constant of 1000 kJ $mol^{-1}nm^{-2}$). The electrostatic and dispersive interactions were calculated with the particle mesh Ewald method [47,48] and with the Lennard-Jones potential (limited to 9 Å) [49], respectively. Temperature and pressure were held constant at 300 K and 1 bar, respectively, using YASARA's default temperature and pressure control settings. Simulation frames were extracted every 0.5 ps to ensure solvent settings were not reasonably correlated. The remaining simulation frames were used for the subsequent calculation of the Radius of Gyration (Rg) and the SWAXS curve. The number of frames was calculated with the formula $2e^5$/N-0.77, where N is the (approximate) number of atoms in the shell. All MD simulations and further adjustments were carried out using the WAXSiS (Wide Angle X-Ray Scattering in Solvent) tool (http://waxsis.uni-goettingen.de/) [50]. For the visualization of the structures, the Molegro Molecular Viewer (MMV)-V.7.0 [51] and BIOVIA Discovery Studio Visualizer [52] software was used.

Additionally, MD simulations were performed to obtain minimum energy conformations and predict potential conformational alterations of the primers. Each MD consisted of three phases that allow sampling trajectories of interest as suggested: relaxation, equilibrium (represented by two runs), and production [53-57]. MD of PDB-format structures of the primers was performed in an explicit water system, solvating the system in an 8.0 Å box. The Amber99SB-ILDN force field [45] and the TIP3P water model [46] were used. Ions were added to the system proportionally to neutralize the overall net charge and to simulate the condition in a 0.15 M physiological aqueous medium. Na^+ and Cl^- ions were introduced for the cationic contribution and anionic effect, respectively. Periodic MD conditions were considered, and Berendsen's algorithm was used to maintain the system at constant temperature and pressure (300 K and 1 bar, respectively). Periodic MD conditions were: an initial steep descent into 5000-step energy mine structures, followed by energy minimization with the 5000-step conjugate gradient approach. Position constraints were applied on the primer atoms, and an initial modeling simulation was performed at 100 ps with the positions of the atoms in the primers constrained by a force constant of 10 kcal/(mol*$Å^2$) in order to allow water molecules to diffuse around the primer and reach equilibrium in the system. The water molecules were treated as rigid bodies, allowing a simulation time step of 2 fs to be performed. To consider the electrostatic contribution to the system, a cutoff of 14.0 Å and a time step of 1 fs were used using the Particle Mesh Ewald (PME) method [47,48]. TIP3P water is suitable for the PME method. Also, the cutoff distance for the Van der Waals contribution was 14.0 Å. After applying the steep descent algorithm to meet the energy minimization of all systems, the canonical NVT set (per 100 ps) was applied with the system thermalized at 300 K.

Subsequently, a second run at 100 ps was applied with the isothermal-isobaric NPT set (to balance the system at 1 bar and 300 K) to obtain the equilibrium of the system. To satisfy the constraints of the link geometry, the SHAKE algorithm with a time step of 2 fs was used [58]. Finally, the production phase was carried out with the NPT assembly following an MD at a constant temperature and pressure (300 K and 1 bar) for a total simulation time of 100 ns. Minimum energy structures in PDB format were extracted every 10 ns as target structures from a 100 ns trajectory to be used in subsequent analyses. The following equation was used for root mean square deviation (RMSD) calculations,

$$RMSD = \sqrt{\frac{1}{n}\sum_{i=1}^{n}\delta_i^2} \qquad \text{Eq. } \mathbf{1}$$

where δ_i is the distance between atom i and a reference structure or the average position of the n equivalent atoms, all MD simulations and additional adjustments were performed using COSGENE/myPresto v5 [59].

2.5. Prediction of the theoretical diffusivity of the primers of interest.

The mobility of biological molecules depends mainly on two factors: 1) the concentration of the crowding macromolecular solutions (related to the viscosity η of the solution), and 2) the relative size of the molecule of interest. In this sense, the size of the primers was calculated in terms of their radius expressed in Angstroms (Å) using the Solvent Accessible Surface Area (SASA) calculation method using the Shrake-Rupley algorithm [60]. The diffusion coefficients of the primers were measured as a function of the macromolecular crowding solution, for which the experimental value of η of the model cell line HeLa (cytoplasmic viscosity of ~4.4×10^{-2} Pa/s) was used (denoted here model 1) [61]. In addition, Normal Swiss 3T3 cells (~2.4×10^{-2} Pa/s viscosity) (designated model 2) were also considered [61,62]. The selection of HeLa and 3T3 cells was carried out to similar the mobility of the primers in solutions of high and normal macromolecular crowding, respectively [61,62]. The translational diffusion coefficient (D_t) was calculated with the Stokes-Einstein equation (equation 2) as suggested [61,62]:

$$D^t = \frac{k_B T}{6\pi\eta R} \qquad \text{Eq. } \mathbf{2}$$

In this model (equation 2), the source of internal friction (dissipative effects) is the η of the simulated medium (cell cytoplasm) [62]. Where k_B is the Boltzmann constant, T is the absolute temperature, η is the viscosity, and R is the radius of the primer. Furthermore, for illustrative purposes, the results of models 1 and 2 were compared with the relative η of water (viscosity of ~0.001 Pa/s) (designated as model 3) to represent a cell-free model (no macromolecular crowding solution) [63]. On the other hand, when taking the mean of the distances in the equation of Phillips *et al*., 2009 [64], which describes the diffusion time (t) of the molecules located at a given point, and taking into account several dimensions (using the Pythagorean theorem), we obtain according to Schavemaker *et al*., 2018 [65] the following equation:

$$t = \frac{d^2}{6nD} \qquad \text{Eq. } \mathbf{3}$$

where d is the distance, n is the number of dimensions considered, and D, the diffusion coefficient with the translational contribution.

2.6. Statistical analyses.

In all the analyses, a comparison of means of the analyzed variables was applied, performing a single-factor analysis of variance (ANOVA) with a confidence interval of 99% (significance level $p < 0.01$) in the case of the comparison of means between analysis groups for each primer. If necessary, Tukey's comparison and separation of means tests were used to see statistical differences (if any) between the means. For the analysis of variance of the analyses by pairs of primers, a t-test was applied for two samples assuming equal variances with a confidence interval of 99% (significance level $p < 0.01$). Percentage representations of measurements were also used. A simple and multiple correlation analysis was also carried out to explore which of the primary variables (thermodynamic and classical dynamic) have greater statistical weight than others to reduce the variables, propose predictors, and establish collinialities. Subsequently, a principal component analysis (PCA) was performed in order to explain the observed variability [66]. The main applications of factor techniques are *i*) *to reduce* the number of variables and *ii*) to *detect structure* in the relationships between variables, that is, to classify variables. Factor loadings are obtained from original (metrics/parameters) variables. Therefore, these factors group most of the characteristics by means of a linear combination of the original elements. Factors defined as consecutive are orthogonal and independent of each other. The first factor obtained tends to be more correlated with the variables than the rest of the factors. This is because the factors are extracted successively, and therefore, they will contribute less to the overall variance. In this sense, one of the most relevant conclusions of this type of multivariate model is that the variables with a high contribution to the same factor will be interrelated the greater their contributions. That is, those features strongly loaded (loading value ≥ 0.7) in the same component (factor) are linearly dependent, whereas variables strongly loaded in different factors are linearly independent. Lastly, the variability/orthogonality analysis was performed using the STATISTICA software (v8.0) [67], and "varimax normalized" was used as a rotational strategy to obtain the factor loadings from the PCA. This rotational type procedure allows obtaining a defined pattern of contributions (loads), high and low for each variable. The method called "normalized varimax" is the most used in order to rotate the variables. This strategy makes the structure of the factors pattern as simple as possible, permitting a clearer interpretation of the factors without loss of orthogonality between them.

3. Results and Discussion

Orthopoxvirus infections cause clinically distinctive skin lesions, yet they can be misdiagnosed. The likelihood of misdiagnosis only increases as time elapses since the last case of smallpox. To improve early detection, the main requirements for laboratory diagnostic tests are rapid results with high sensitivity and specificity.

3.1. Primer design and associated "binding region" annotation.

Quantitative nucleic acid testing has become the gold standard for diagnosis and guiding clinical decisions. However, PCR assays targeting MpxV have several challenges, especially primer design. Primers are the pivotal components of a PCR assay. Some primers have also been made available on the WHO website for reference. However, no previous studies have systematically compared the previously reported genes. We also described how to design new primers for other genes relevant to MpxV infection. It is well known that

amplifying sequences of interest using primers is key, and it should be a standardized process from the start. Primers must seek the highest possible specificity and are susceptible to several factors that can limit the success of PCR reactions, so computational methods represent the first design tools to be optimized.

Firstly, from the NCBI/GenBank Primer3-BLAST algorithm [35], 30 pairs of specific primers (Table S1 and Figure S1) aimed at the *in silico* amplification of the OPG191, OPG117, OPG118, OPG032, OPG035, OPG047, OPG190 and OPG200 genes of the MpxV were identified for a total of 240 nucleotide sequences (8 genes × 30 primers). The Representative Genome Database was considered for the design, considering representative genomes of the MpxV (Table S2). The BLAST tool was used to validate the similarity of the sequences with the nucleotide collection through the standard database search. All the pairs of designed primers presented a percentage of identity and a query coverage of 100% and 0% of gaps against sequences associated with MpxV.

Secondly, from the MFEprimer algorithm [22], the thermodynamic stability and specificity of the previously predicted sequences were reclassified, and 8 thermodynamically stable primer pairs (one pair for each gene of interest) were selected, which did not generate dimers or hairpin-like conformations and with the highest theoretical specificity predicted under reclassification. Specifically, for the reclassified primers, a mean number of potential amplicons of ≈77 was predicted, with a minimum of 27 and a maximum of 188, represented by the pair of primers targeting the OPG200 and OPG047 genes, respectively. From the 8 selected primer pairs, a total of 662 potential amplicons were predicted, of which ≈71% (474/622) corresponded to MpxV amplicons. However, potential off-target amplicons with theoretical activity were also predicted cross for *Vaccinia virus* (104/662), *Cowpox virus* (22/622), *Ectromelia virus* (10/662), *Camelpox virus* (5/622), *Horsepox virus* (2/622), *Taterapox virus* (2/622), *Rabbitpox virus* (2/622) and *Buffalopox virus* (1/622). Specifically, the predicted primer pairs with potential cross-reactions were those targeting the genes OPG047 with ≈64%% (122/188), OPG032 with ≈24% (21/86), and OPG035 with ≈8% (5/62). At the same time, the primers directed to the genes OPG190, OPG200, OPG191, OPG190, and OPG117 did not show theoretical cross-reactions under the conditions of this study. These results show the usefulness of these targets for the potential detection of a wide group of genera; simultaneously, combinations could be made to carry out multiple detection assays, as has been reported [10,11]. None of the assays showed cross-reactions with human DNA as expected [36,68], except the primers to OPG047 and OPG200. It is important to point out that the model for calculating thermodynamic stability based on DNA folding predicted that the primers targeting the OPG047 and OPG200 genes are part of the thermodynamically less favorable primers (Table 2). The models used here that consider the thermodynamic modeling criterion for primer formation predicted that all primer sequences studied are thermodynamically stable with a $\Delta G \approx -23$ kcal/mol, with a minimum value of -26 kcal/mol and a maximum of -21 kcal/mol ($t = 23.188$, $GL = 30$, $p < 0.0001$, $\alpha = 0.01$), and a Tm with a mean of 62 ˚C, with minimum values of Tm ≈ 58 ˚C and a maximum of Tm ≈ 66 ˚C ($F[2,45] = 73.841$, $p < 0.0001$, $\alpha = 0.01$). These parameters were mediated predominantly by the entropy effect as predicted and are indicative of favorable and spontaneous conformations.

Table 2. Thermodynamic stability and dynamic parameters of primers for the specific detection of MpxV.

Primer ID	MFEprimer		FastPCR					DNAFold[a]				Rg	RMSD	ε^c
	ΔG	Tm	ΔG	ΔH	ΔS	Tm	Tm	ΔG	ΔH	ΔS	Tm[b]			
	[kcal/mol]	[°C]	[kcal/mol]		[cal/(K·mol)]	[°C]		[kcal/mol]		[cal/(K·mol)]	[°C]	[Å]		[%]
P1 - OPG191	-22.0	60.6	-25.7	-153.4	-431.9	63.2	64.4	-1.3	-27.3	-83.7	52.6	20.0	1.8	83
P1 - OPG117	-22.3	60.5	-25.9	-158.1	-446.1	62.8	64.4	-0.2	-36.2	-116.2	38.3	20.2	2.4	77
P1 - OPG118	-21.8	59.6	-25.4	-157.1	-444.4	61.6	62.3	0.6	-4.5	-16.5	-1.0	20.2	2.4	71
P1 - OPG032	-21.4	58.0	-25.1	-160.7	-457.9	60.1	62.6	-0.3	-35.6	-113.8	39.4	21.0	2.5	90
P1 - OPG035	-22.0	60.1	-25.7	-156.1	-440.6	62.6	64.4	-0.2	-21.9	-69.9	40.1	20.2	2.6	87
P1 - OPG047	-22.8	60.3	-26.6	-166.5	-471.9	62.3	64.6	0.4	-14.5	-47.9	29.0	20.6	3.0	85
P1 - OPG190	-21.8	59.8	-25.4	-155.3	-438.6	62.0	62.3	-0.4	-23.7	-75.1	42.0	20.0	2.3	71
P1 - OPG200	-22.0	60.2	-25.6	-155.6	-439.0	62.3	62.3	-0.03	-23.3	-75.0	37.3	20.0	3.1	87
P2 - OPG191	-22.4	60.0	-26.2	-162.3	-459.8	62.3	64.6	-1.3	-31.3	-96.6	50.5	20.9	2.4	87
P2 - OPG117	-21.8	60.2	-25.3	-151.7	-427.3	63.0	64.4	0.3	-17.1	-56.1	31.3	20.1	2.2	68
P2 - OPG118	-21.8	59.6	-25.4	-156.0	-441.0	61.7	62.3	-1.3	-44.3	-138.5	46.6	20.2	2.5	95
P2 - OPG032	-21.3	60.7	-24.6	-142.0	-396.6	63.6	64.0	-1.4	-31.6	-97.3	51.4	18.3	2.1	66
P2 - OPG035	-22.3	60.7	-26.0	-157.0	-442.5	63.1	64.4	-0.2	-21.8	-69.6	39.8	20.2	2.5	84
P2 - OPG047	-21.4	59.2	-25.0	-152.7	-431.7	61.9	64.4	1.3	-6.7	-25.7	-13.3	20.1	2.4	82
P2 - OPG190	-22.1	59.5	-25.6	-160.7	-455.3	61.6	64.4	0.7	-11.4	-39.0	18.8	20.1	1.5	79
P2 - OPG200	-21.9	60.1	-25.5	-154.7	-436.5	62.9	66.4	0.8	-20.7	-69.3	25.3	20.5	2.5	58

[a], thermodynamics of folding at 37 °C. Linear DNA folding and ionic conditions: [Na^+] = 1.0 M. Standard errors are roughly ±5%, ±10%, ±11% and 2-4 °C for free energy (ΔG), enthalpy (ΔH), entropy (ΔS) and Tm, respectively; [b], assuming a 2 state model; [c], efficiencies in the PCR reactions to FastPCR [25,38,39].

Both the MFEprimer and FastPCR models predicted a reproducible and correlated minimum free energy of formation (MFE) of primers ($R^2 = 0.99$), and in terms of the difference between the ΔG of each pair of primers, a mean ΔΔG was predicted ≈ -0.07 kcal/mol, with a minimum value of 0 kcal/mol and a maximum of -1.6 kcal/mol. However, despite the significant difference in thermodynamic means and Tm, these predictions did not allow us to clearly discriminate between thermodynamically more stable primer pairs from less stable ones, especially since, according to these approaches, 88% (7/8) of the primer pairs had the same Gibbs minimum free energy for their formation. Specifically, of the pairs of primers studied, 75% (6/8) presented a ΔG ≈ - 22 kcal/mol (Table 2).

On the other hand, with the approach based on the thermodynamic study of the biomolecular folding of the individual primers, a mean of ΔG ≈ - 0.2 kcal/mol was predicted, with a minimum value of -1.4 kcal/mol and a maximum of 1.3 kcal/mol, represented by primer P2 - OPG032, and primer P2 - OPG047, respectively. These results also represented values with a significant difference with respect to those predicted by the previous models (MFEprimer and FastPCR) ($F [2,45] = 8229.253$, $p < 0.0001$, $\alpha = 0.01$). However, at the molecular level, only ≈63% (10/16) of the primers were predicted to have a thermodynamically favorable folding. In addition, of the group of primers with a negative Gibbs minimum free energy, 40% (4/10) presented a ΔG ≥ -1 kcal/mol. These observations are important because they show that the considered sequences tend to maintain their unfolded conformation, avoiding the formation of hairpin-loops-like structures as previously predicted. Additionally, it was observed that from a ΔS < -69 cal/(K mol), the entropic contribution of the primers tends to decrease to a level that modifies the thermodynamic stability of the biomolecule and with a final impact at the Tm level. These predictions allow us to validate that the entropic contribution of these systems determines the primers' stability. In this sense, and according to the thermodynamic folding approach at constant temperature (*via* DNA fold), only the primers directed to the B7R gene (P1 - OPG191 and P2 - OPG191) presented an optimal Tm (≈ 50 ˚C) together with stability in thermodynamic folding at 37 ˚C (specifically -1.3 kcal/mol each) (Table 2). Therefore, secondary structures with similar conformations, typical of stable sequences with little structural deformability, were predicted. The comparative analysis between the secondary structures of the primers showed a significant degree of conservation of the sequences in terms of structural stability and conformation, despite being non-consensual sequences. It is important to note that the structures predicted for the OPG191 primer pair exhibited similar conformations (Figure 1).

The *in silico* PCR reaction with the FastPCR algorithm [25,36,37] predicted an overall efficiency of the reactions mediated by these primers of ≈80%, with a minimum efficiency of ≈73% (primers for the OPG117 and OPG200 gene) and a maximum of ≈86% (for the OPG191 and OPG035 gene). The efficiencies in the theoretical PCR reactions for the OPG032, OPG118, and OPG200 genes were decreased by 24%-29% because of at least one primer, especially for the reverse type sequences (Table 2).

Typical scattering curves are shown in Figure 3a. The shape of the curves allows for several qualitative information to be extracted [69]; for example, the bending of the curve at low q-values indicates the existence of structures about 30 to 100 Å. Although the variations in the length of the primers (that ranged between 21 – 18 nt) could be seen reflected in the trajectories of the spectra predicted by the SWAXS-driven MD approach (especially for the primers directed to the OPG032 gene), in general, the fluctuations in the spectra were similar with some primers with a theoretical tendency to aggregation or folding due to the decrease in

the intensity of the signals of the transitions, such as P2 - OPG047, P2 - OPG190 and P2 - OPG200. Interestingly, in this group of primers, some of the least favorable thermodynamically in terms of ΔG at constant temperature were predicted, with less specificity than the rest. MD in explicit solvent showed stable structures (RMSD ≈ 2.5 Å) (Figure 3c) without significant differences (t = 1.315, GL = 14, p = 0.209, α = 0.01), as well as similar conformational folds between the pairs of primers studied (t = 0.765, GL = 14, p = 0.456, α = 0.01) with a mean of Rg ≈ 20 Å (Figure 3b), and with minimum values of Rg = 18.31 Å and a maximum of Rg = 21.01 Å.

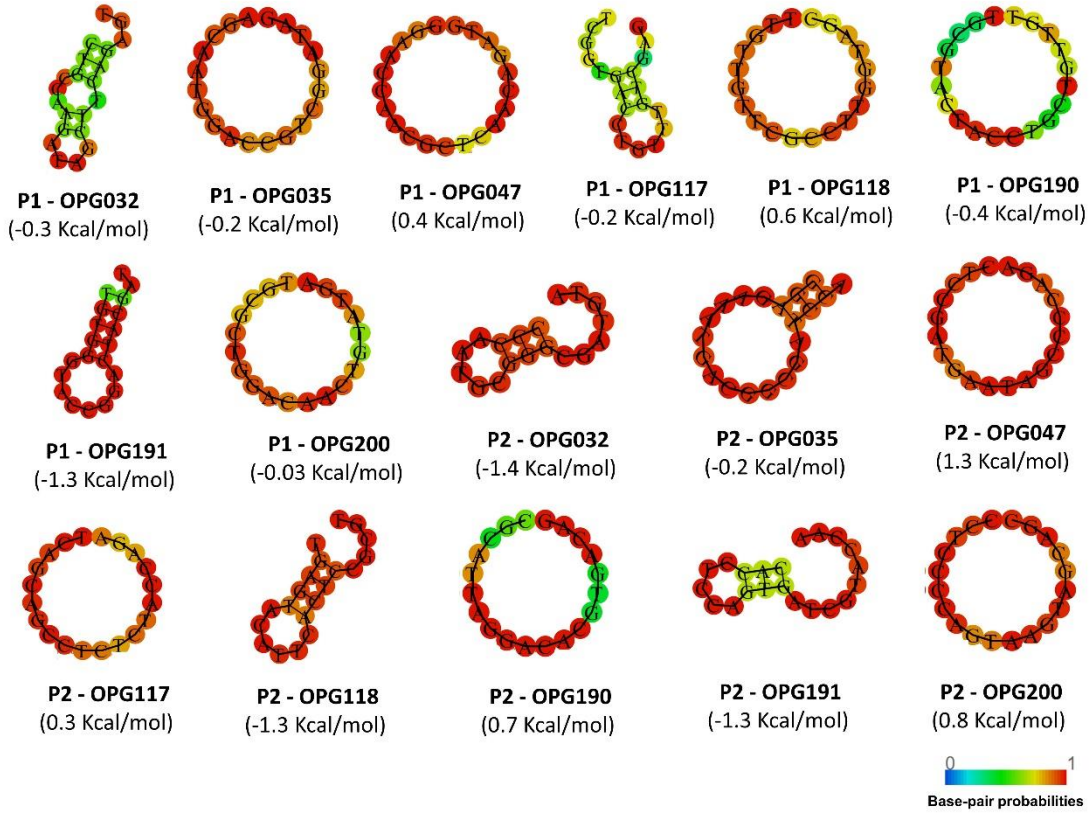

Figure 1. Secondary structures of the nucleotide sequences associated with primers directed to the specific detection of MpxV.

Interestingly, these radii correspond to the primers P2 - OPG032 and P1 - OPG032, targeting the OPG032 gene, respectively, showing a ΔRg ≥ 3 Å (Figure 3d, 2e, 2f), which may be associated with the difference in the length of the primers. Rg is related to the scatterer's size and shape [70]. Results show a differential behavior in the conformational fluctuation of this type of primer in an aqueous medium, which in turn corresponds to the differences in the predictions of the reaction efficiency. In fact, it has been described that geometrical features of DNA, such as the interhelical spacing, result in clearly discernible diffraction peaks, which can be used to quantify their geometry. Also, SAXS can quantify the equilibrium distribution of conformational states providing useful thermodynamic information, including the dependence of the folding of DNA structures and interhelical spacing on temperature and the concentration of ions [69].

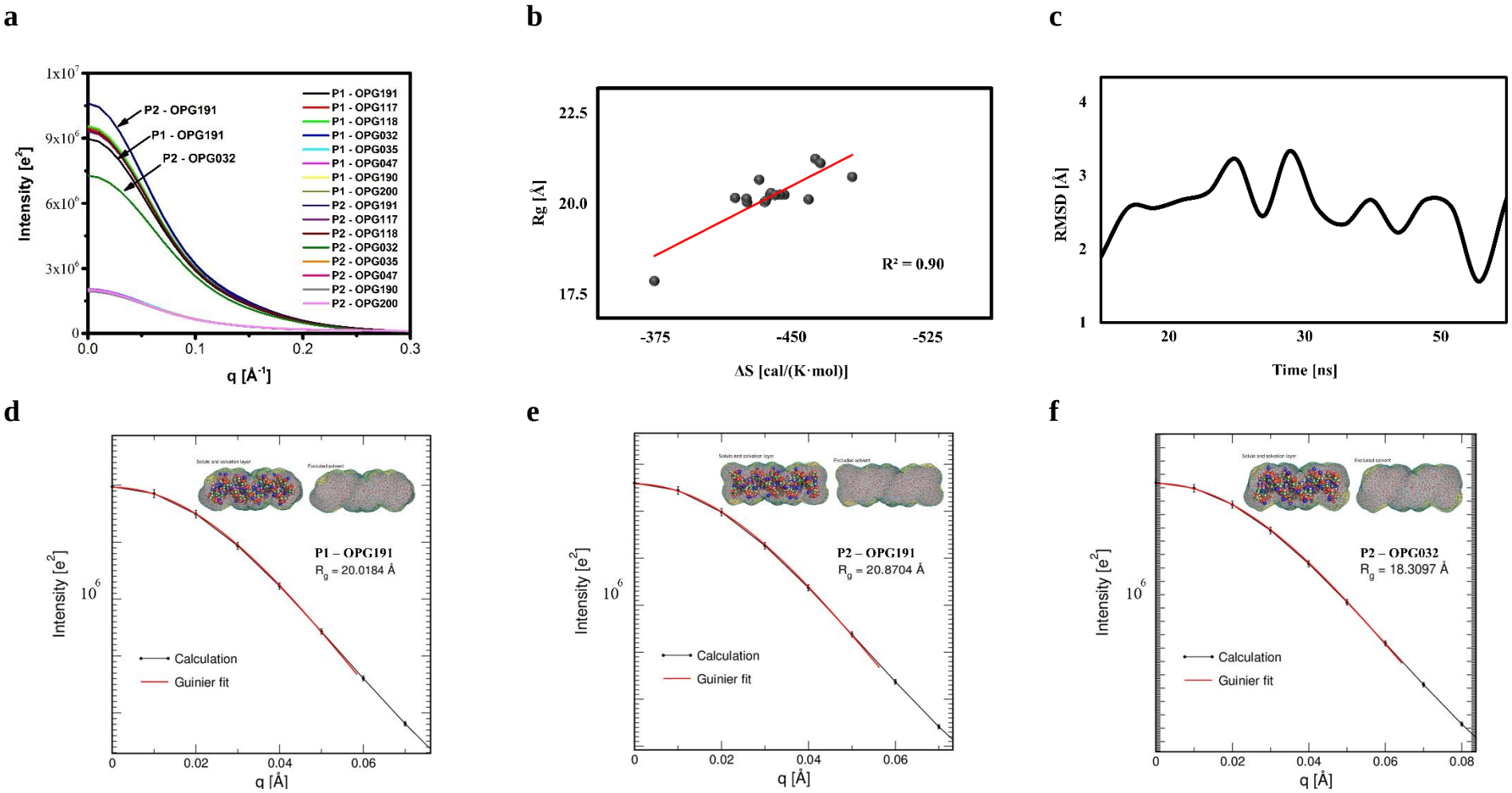

Figure 3. Thermodynamic and dynamic stability of primers for the potential specific detection of MpxV. **a**) predicted spectra for the primers with the SWAXS-curves-based MD approach [50], **b**) Gyration radii (Rg) and ΔS, **c**) RMSD at 50 ns, **d)** and **e**) Guinier plot to primers for the OPG191, and **f**) OPG032, respectively.

The primers' ability to move in artificial environments was studied by simulating various types of cytoplasmic congestion, with the interest of observing the diffusion of primers. In this sense, and after studying two conditions of congestion and an aqueous model, a minimum translational diffusion coefficient (D^t) of 3.4×10^{-12} cm^2 s^{-1} and a maximum of D^t = 4.0×10^{-12} cm^2 s^{-1} was predicted for the cellular models, in contrast to a minimum of D^t = 1.04×10^{-10} cm^2 s^{-1} and a maximum of D^t = 1.20×10^{-10} cm^2 s^{-1} for the aqueous model. Although all the diffusion values ($F_{[2,45]} = 15004.49$, $p < 0.0001$, $\alpha = 0.01$), including the diffusion times between the studied primers ($F_{[2,45]} = 6979.51$, $p < 0.0001$, $\alpha = 0.01$), were very close, significant differences in their means were predicted. A high negative correlation was also predicted between the entropic contribution of the primers in the *in silico* PCR reaction (according to the FastPCR algorithm [25,36,37]) and the decrease in the diffusion of the primers in artificial and aqueous cell media (R^2 = -0.90). These predictions are important because the primers showed similar behavior and trend regardless of the simulated medium, which indicates that their conformational changes due to the effect of the simulation period do not significantly alter the diffusion of biomolecules. An aspect that has proven to be very important if one seeks to characterize the dynamic behavior of biomolecules [60,71].

Table 3. Comparative analysis of the theoretical translational diffusion coefficient and the diffusion time of the primers of interest.

Primer ID			D^t (cm^2 s^{-1})			*t* (sec)		
	MW (g/mol)	*r* (Å)	Model 1[a]	Model 2[a]	Model 3[b]	Model 1[c]	Model 2[c]	Model 3[c]
P1 - OPG191	6173	20.0	2.49	4.57	1.09	2.4	1.3	5.5
P1 - OPG117	6155	20.2	2.47	4.53	1.08	2.4	1.3	5.6
P1 - OPG118	6121	20.2	2.47	4.53	1.08	2.4	1.3	5.6
P1 - OPG032	6430	21.0	2.38	4.37	1.04	2.5	1.4	5.8
P1 - OPG035	6191	20.2	2.48	4.54	1.08	2.4	1.3	5.6
P1 - OPG047	6433	20.6	2.43	4.45	1.06	2.5	1.3	5.7
P1 - OPG190	6090	20.0	2.49	4.57	1.09	2.4	1.3	5.5
P1 - OPG200	6157	20.0	2.49	4.57	1.09	2.4	1.3	5.5
P2 - OPG191	6335	20.9	2.39	4.39	1.05	2.5	1.4	5.7
P2 - OPG117	6022	20.1	2.48	4.55	1.09	2.4	1.3	5.5
P2 - OPG118	6068	20.2	2.47	4.52	1.08	2.4	1.3	5.6
P2 - OPG032	5525	18.3	2.72	5.00	1.20	2.2	1.2	5.0
P2 - OPG035	6200	20.2	2.47	4.54	1.08	2.4	1.3	5.6
P2 - OPG047	6071	20.1	2.48	4.56	1.09	2.4	1.3	5.5
P2 - OPG190	6151	20.1	2.49	4.56	1.09	2.4	1.3	5.5
P2 - OPG200	6047	20.5	2.43	4.46	1.07	2.5	1.3	5.6

D_t, translational diffusion coefficient. Model 1, HeLa (~4.4×10^{-2} Pa/s) [63]; Model 2, Normal Swiss 3T3 cells (~2.4×10^{-2} Pa/s) [61,62]; Model 3, standard viscosity of water (~1.0×10^{-3} Pa/s) [63]. [a], all values are at 10^{-12}; [b], all values are at 10^{-10}; [c], all values are at 10^{-4}.

Additionally, a high negative correlation was also predicted between the decrease in the entropic contribution of the primers in the *in silico* PCR reaction (according to the FastPCR algorithm [25,36,37] and the decrease in the conformational folding fluctuation of the primers in aqueous medium and as a function of time simulation (R^2 = -0.90) (Figure 3b). These observations correspond to the PCA results, in which it was found that 80.7% of the variability observed in the primers designed and selected after reclassification can be explained by the effect of the interaction between the thermodynamic stability of the primers and their conformational fluctuations in solution (PC1, PC2 and PC3), which could impact the efficiency of predicted PCR reactions (Table S3, Table S4, Table S5). Table S5 shows the factor loadings [varimax normalized rotation] for variables of the 8 forward and reverse primers).

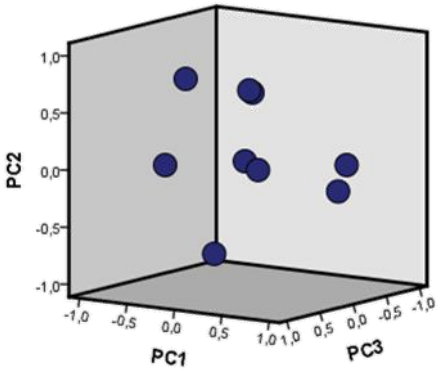

Figure 3. Plot of components in rotated space of the variables associated with thermodynamic stability and dynamic parameters of primers for the specific detection of MpxV.

The results of the factor analysis are summarized as Supporting Information (Table S5), and the 5 principal factors explain approximately 92% of the total variance. The first factor explains 48.1% of the variance in the variables studied. The addition of the second-factor increases 66.1% of the variance explained, and the addition of the third factor allows 80.7% of the variance of the features to be accounted for (Table S5). After a Varimax normalized rotation of the factors, factor loadings from the principal component analysis are shown in Table S5. Specifically, the predictions with the multivariate model showed that the DNAfold metrics are orthogonal to most of the FastPCR parameters, which corresponds to the discriminating thermodynamic capacity of the DNAfold approach.

It is important to highlight that the prediction of the primers' stability based on the folding's thermodynamics allowed us to discriminate more clearly the contribution of the thermodynamic parameters in the primers, which were predicted with similar stability by the rest of the methods used. In addition, although the most thermodynamically stable primers showed differences of only 1 kcal/mol (according to the DNA folding method), it has been reported that even a small number of non-binding bases is sufficient to increase the free energy of hybridization in about 1 kcal/mol at physiological salt concentrations [72]. It is known that the contribution of base pair mismatches to DNA stability can range from 1 kcal/mol to 2 kcal/mol. Furthermore, variations in pH can contribute to imbalances ranging from 1 kcal/mol to -0.4 kcal/mol [73].

In this sense and considering that the resulting predictors associated with thermodynamic stability and conformational fluctuations can be decisive in the theoretical efficiency of the PCR reaction, it is suggested, under the conditions of this study, to consider MpxV-specific primers such as those designed and selected for targeting the OPG191 gene (Table 2, Table 4) for optimal characteristics in terms of thermal and dynamic stability. Furthermore, for illustrative purposes, and by examining the thermodynamic stability of the OPG191 primers at 95 ˚C, as is a common condition in these reactions [6], the stability of the biomolecule, which does not undergo conformational changes at this temperature was confirmed, such as the formation of thermodynamically favorable hairpin-loops (Figure S2). In addition, it is important to note that all the primer sequences studied could form secondary structures with minimum free energies (MFE) of assembly that are thermodynamically highly spontaneous, as reported for nucleotide sequences of similar sizes [74].

Table 4. Proposed primers for the detection of Monkeypox virus (MpxV).

Assay/use =	**B7R gene (OPG191)***
P1 - OPG191 =	P2 - OPG191 =

Assay/use =	**B7R gene (OPG191)***
5'-TGTGGGTACCGGACTACGAT-3'	5'-CACCTCCAGTGATCGTACCAA-3'
Extinction coefficient = 194400 L/(mol·cm) Molecular weight = 6173 g/mol OD260 = 1.000 µg = 31.754 nmol = 5.144 100µM = dissolve in 51.4 µl of MQ-water or TE buffer	Extinction coefficient = 200100 L/(mol·cm) Molecular weight = 6335 g/mol OD260 = 1.000 µg = 31.659 nmol = 4.998 100µM = dissolve in 50.0 µl of MQ-water or TE buffer
Product Size (bp) =	≈ 236

*all calculations for the theoretical PCR reaction were generated using the MFEprimer and server and the FastPCR tool.

It is important to highlight that to distinguish between these infections, particularly if MpxV is suspected, the main requirements for laboratory diagnostic tests are rapid results with high sensitivity and specificity. The most recent advance in the rapid diagnosis of Orthopoxvirus infection has been provided by polymerase chain reaction (PCR) assay. For this reason, the OPG191 gene has been suggested as appropriate for identification tests. It has even been recommended to differentiate MpxV and other related viruses [11]. Likewise, carrying out the PCR reaction (with the proposed primers) is recommended using the previously reported control primers to detect MpxV [13,73-78].

Our recommendations are since the approach proposed here reproduced the thermodynamic stability of the molecular folding of the published primers for detecting MpxV by PCR. Specifically, the thermodynamic trend in terms of the entropic contribution and the minimum free energy for the formation of the OPG035 and OPG191 primer pair was similar for both the published and predicted primers in this study. Furthermore, the thermodynamic discrimination between the published primers in terms of entropic contribution was like that predicted in this study (Table S4). These results allow us to infer that the primers directed to genes associated with MpxV present a similar thermodynamic stability governed by a negative entropic contribution, especially for the primers predicted from the OPG035 and OPG191 genes. The negative entropic contribution is a phenomenon that has already been described for other unrelated short nucleotide sequences of prokaryotic [79,80] and eukaryotic origin [81-84].

This study does not intend to indicate which target is the most suitable for the design of primers directed at MpxV, nor does it intend to invalidate any of the primers designed with the proposed tools. This study sought to propose an alternative strategy to characterize and discriminate primers considering the thermodynamics of molecular folding and molecular dynamics, to optimize the predictions of *in silico* PCR reactions at the thermodynamic level from a biophysical-computational point of view, as suggested [85-88]. In this sense, experimental demonstrations are required to study the impact of primer fold stability on the efficiency of PCR reactions, including variables such as mismatches and their effect on annealing temperatures [89,90].

4. Conclusions

Using standard predictors, several thermodynamically stable and specific primers were designed targeting reported genes of interest for MpxV detection. Differences were observed between the thermodynamic stability of the previously designed primers by means of a subsequent classification based on the prediction of DNA folding at a constant temperature. Differences in terms of specificity were also predicted after applying quality control with additional alternative tools that rank primers by performing searches that consider

thermodynamic stability. We reclassified primers that could be directed to the specific detection of MpxV, or the amplification of sequences of interest from a diverse group of Orthopoxviruses. A relationship was observed between the thermodynamic stability and the conformational fluctuations of the primers in an aqueous medium after the molecular dynamics analysis and a possible effect of these variables on the theoretical efficiency of the PCR reactions. Finally, under the conditions of this study, it is suggested to carry out experimental demonstrations for the specific detection of MpxV considering primers such as those characterized in this study, which is directed to the OPG191 gene, for presenting optimal characteristics in terms of thermal and dynamic stability.

Funding

This research did not receive any specific grant from public, commercial, or not-for-profit funding agencies.

Acknowledgments

This research has no acknowledgment.

Conflicts of Interest

The authors declare that they have no known competing financial interests or personal relationships that could have appeared to influence the work reported in this paper.

References

1. Senkevich, T. G.; Yutin, N.; Wolf, Y. I.; Koonin, E. V.; Moss, B. Ancient Gene Capture and Recent Gene Loss Shape the Evolution of Orthopoxvirus-Host Interaction Genes. *Mbio.* **2021**, *12*, e01495-21; https://doi.org/10.1128/mBio.01495-21.
2. Pauli, G.; Blümel, J.; Burger, R.; Drosten, C.; Gröner, A.; Gürtler, L.; von Koenig, C. H. Orthopox viruses: infections in humans. *Transfusion Medicine and Hemotherapy* **2010**, *37*, 351. https://doi.org/10.1159/000322101.
3. Babkin, I. V.; Babkina, I. N. The origin of the variola virus. *Viruses* **2015**, *7*, 1100-1112, https://doi.org/10.3390/v7031100.
4. Mauldin, M. R.; McCollum, A. M.; Nakazawa, Y. J.; Mandra, A.; Whitehouse, E. R.; Davidson, W.; Reynolds, M. G. Exportation of monkeypox virus from the African continent. *The Journal of infectious diseases* **2022**, *225*, 1367-1376, https://doi.org/10.1093/infdis/jiaa559 .
5. Likos, A. M.; Sammons, S. A.; Olson, V. A.; Frace, A. M.; Li, Y.; Olsen-Rasmussen, M.; Damon, I. K. A tale of two clades: monkeypox viruses. *Journal of General Virology* **2005**, *86*, 2661-2672, https://doi.org/10.1099/vir.0.81215-0.
6. Li, Y.; Olson, V. A.; Laue, T.; Laker, M. T.; Damon, I. K. Detection of monkeypox virus with real-time PCR assays. *Journal of Clinical Virology* **2006**, *36*, 194-203, https://doi.org/10.1016/j.jcv.2006.03.012.
7. Kumar, N.; Acharya, A.; Gendelman, H. E.; Byrareddy, S. N. The 2022 outbreak and the pathobiology of the monkeypox virus. *Journal of Autoimmunity* **2022**, *131*, 102855, https://doi.org/10.1016/j.jaut.2022.102855.
8. Taylor, L. Monkeypox: WHO to rename disease to prevent stigma. *BMJ* **2022**, *377*, https://doi.org/10.1136/bmj.o1489.
9. 9.- Rodriguez-Morales, A. J., Lopardo, G. Monkeypox: another sexually transmitted infection?. *Pathogens* **2022**, *11*, 713, https://doi.org/10.3390/pathogens11070713.
10. Guarner, J.; Del Rio, C.; Malani, P. N. Monkeypox in 2022—what clinicians need to know. *Jama* **2022**, *328*, 139-140, https://doi.org/10.1001/jama.2022.10802.
11. Shchelkunov, S. N.; Shcherbakov, D. N.; Maksyutov, R. A.; Gavrilova, E. V. Species-specific identification of variola, monkeypox, cowpox, and vaccinia viruses by multiplex real-time PCR assay. *Journal of virological methods* **2011**, *175*, 163-169, https://doi.org/10.1016/j.jviromet.2011.05.002.
12. Li, Y.; Zhao, H.; Wilkins, K.; Hughes, C.; Damon, I. K. Real-time PCR assays for the specific detection of monkeypox virus West African and Congo Basin strain DNA. *Journal of virological methods* **2010**, *169*, 223-227, https://doi.org/10.1016/j.jviromet.2010.07.012.

13. Falendysz, E. A.; Lopera, J. G.; Doty, J. B.; Nakazawa, Y.; Crill, C.; Lorenzsonn, F., Rocke, T. E. Characterization of Monkeypox virus infection in African rope squirrels (Funisciurus sp.). *PLoS neglected tropical diseases* **2017**, *11*, e0005809, https://doi.org/10.1371/journal.pntd.0005809 .
14. Weiner, Z. P., Salzer, J. S., LeMasters, E., Ellison, J. A., Kondas, A. V., Morgan, C. N., Hutson, C. L. Characterization of Monkeypox virus dissemination in the black-tailed prairie dog (Cynomys ludovicianus) through *in vivo* bioluminescent imaging. *Plos one* **2019**, *14*, e0222612, https://doi.org/10.1371/journal.pone.0222612.
15. World Health Organization. Laboratory testing for the monkeypox virus: interim guidance, 23 May 2022. *World Health Organization*, 2022, 6, https://apps.who.int/iris/handle/10665/354488.
16. Yinka-Ogunleye, A.; Aruna, O.; Dalhat, M.; Ogoina, D.; McCollum, A.; Disu, Y.; Satheshkumar, P. S. Outbreak of human monkeypox in Nigeria in 2017–18: a clinical and epidemiological report. *The Lancet Infectious Diseases* **2019**, *19*, 872-879, https://doi.org/10.1016/S1473-3099(19)30294-4.
17. Reynolds, M. G.; Carroll, D. S.; Olson, V. A.; Hughes, C.; Galley, J.; Likos, A.; ... Damon, I. K. A silent enzootic of an orthopoxvirus in Ghana, West Africa: evidence for multi-species involvement in the absence of widespread human disease. *The American journal of tropical medicine and hygiene* **2010**, *82*, 746, https://doi.org/10.4269%2Fajtmh.2010.09-0716.
18. Orba, Y.; Sasaki, M.; Yamaguchi, H.; Ishii, A.; Thomas, Y.; Ogawa, H.; Sawa, H. Orthopoxvirus infection among wildlife in Zambia. *Journal of General Virology* **2015**, *96*, 90-394, https://doi.org/10.1099/vir.0.070219-0
19. Davi, S. D.; Kissenkötter, J.; Faye, M.; Böhlken-Fascher, S.; Stahl-Hennig, C.; Faye, O.; Abd El Wahed, A. Recombinase polymerase amplification assay for rapid detection of Monkeypox virus. *Diagnostic Microbiology and Infectious Disease* **2019**, *95*, 41-45. https://doi.org/10.1016/j.diagmicrobio.2019.03.015.
20. Maksyutov, R. A.; Gavrilova, E. V.; Shchelkunov, S. N. Species-specific differentiation of variola, monkeypox, and varicella-zoster viruses by multiplex real-time PCR assay. *Journal of virological methods* **2016**, *236*, 215-220, https://doi.org/10.1016/j.jviromet.2016.07.024.
21. Ropp, S. L.; Jin, Q. I.; Knight, J. C.; Massung, R. F.; Esposito, J. J. PCR strategy for identification and differentiation of small pox and other orthopoxviruses. *Journal of clinical microbiology* **1995**, *33*, 2069-2076, https://doi.org/10.1128/jcm.33.8.2069-2076.1995.
22. Corman, V. M.; Landt, O.; Kaiser, M.; Molenkamp, R.; Meijer, A.; Chu, D. K.; ... Drosten, C. Detection of 2019 novel coronavirus (2019-nCoV) by real-time RT-PCR. *Eurosurveillance* **2020**, *25*, 2000045, https://doi.org/10.2807/1560-7917.ES.2020.25.3.2000045.
23. Parker, S.; Nuara, A.; Buller, R. M.; Schultz, D. A. Human monkeypox: an emerging zoonotic disease. *Future microbiology* **2007**, *2*, 17-34, https://doi.org/10.2217/17460913.2.1.17.
24. Kalendar, R.; Lee, D.; Schulman, A. H. Java web tools for PCR, *in silico* PCR, and oligonucleotide assembly and analysis. *Genomics* **2011**, *98*, 137-144, https://doi.org/10.1016/j.ygeno.2011.04.009.
25. Kalendar, R.; Tselykh, T. V.; Khassenov, B.; Ramanculov, E. M. Introduction on using the FastPCR software and the related java web tools for PCR and oligonucleotide assembly and analysis. *In PCR; Domingues, L. Ed.;* Springer: New York, NY, **2017**, *1620*, 33-64, https://doi.org/10.1007/978-1-4939-7060-5_2.
26. Branco, I.; Choupina, A. Bioinformatics: new tools and applications in life science and personalized medicine. *Applied microbiology and biotechnology* **2021**, *105*, 937-951, https://doi.org/10.1007/s00253-020-11056-2.
27. Kalendar, R. *A guide to using FASTPCR software for PCR, in silico PCR, and oligonucleotide analysis*; PCR Primer Design: New York, NY, USA. **2022**, 223-243, https://doi.org/10.1007/978-1-0716-1799-1_16.
28. Eric, S. D., Nicholas, T. D., & Theophilus, K. A. Bioinformatics with basic local alignment search tool (BLAST) and fast alignment (FASTA). *Journal of Bioinformatics and sequence analysis* **2014** , 6(1), 1-6. https://doi.org/10.5897/IJBC2013.0086.
29. Mann, T.; Humbert, R.; Dorschner, M.; Stamatoyannopoulos, J.; Noble, W. S. A thermodynamic approach to PCR primer design. *Nucleic acids research* **2009**, *37*, e95-e95, https://doi.org/10.1093/nar/gkp443.
30. Qu, W.; Zhou, Y.; Zhang, Y.; Lu, Y.; Wang, X.; Zhao, D.; ... Zhang, C. MFEprimer-2.0: a fast thermodynamics-based program for checking PCR primer specificity. *Nucleic acids research* **2012**, *40*, W205-W208, https://doi.org/10.1093/nar/gks552.
31. Untergasser, A.; Cutcutache, I.; Koressaar, T.; Ye, J.; Faircloth, B. C.; Remm, M.; Rozen, S. G. Primer3—new capabilities and interfaces. *Nucleic acids research* **2012**, *40*, e115-e115, https://doi.org/10.1093/nar/gks596.
32. Untergasser, A.; Nijveen, H.; Rao, X.; Bisseling, T.; Geurts, R.; Leunissen, J. A. Primer3Plus, an enhanced web interface to Primer3. *Nucleic acids research* **2007**, *35*, W71-W74, https://doi.org/10.1093/nar/gkm306.
33. Shchelkunov, S. N.; Gavrilova, E. V.; Babkin, I. V. Multiplex PCR detection and species differentiation of orthopoxviruses pathogenic to humans. *Molecular and cellular probes* **2005**, *19*, 1-8, https://doi.org/10.1016/j.mcp.2004.07.004.
34. Luciani, L.; Inchauste, L.; Ferraris, O.; Charrel, R.; Nougairède, A.; Piorkowski, G.; ... Priet, S. A novel and sensitive real-time PCR system for universal detection of poxviruses. *Scientific reports* **2021**, *11*, 1-6, https://doi.org/10.1038/s41598-021-81376-4.

35. Ye, J.; Coulouris, G.; Zaretskaya, I.; Cutcutache, I.: Rozen, S.; Madden, T. L. Primer-BLAST: a tool to design target-specific primers for polymerase chain reaction. *BMC bioinformatics* **2012**, *13*, 1-11, https://doi.org/10.1186/1471-2105-13-134.
36. Kalendar, R.; Lee, D.; Schulman, A. H. *FastPCR software for PCR, in silico PCR, andoligonucleotide assembly and analysis*; DNA cloning and assembly methods: *Totowa, NJ, USA*, **2014**, 271-302, https://doi.org/10.1007/978-1-62703-764-8_18.
37. Kalendar, R.; Khassenov, B.; Ramankulov, Y.; Samuilova, O.; Ivanov, K. I. FastPCR: An *in silico* tool for fast primer and probe design and advanced sequence analysis. *Genomics* **2017**, *109*, 312-319, https://doi.org/10.1007/978-1-62703-764-8_18.
38. Gruber, A. R.; Lorenz, R.; Bernhart, S. H.; Neuböck, R.; Hofacker, I. L. The vienna RNA websuite. *Nucleic acids research* **2008**, *36*, W70-W74, https://doi.org/10.1093/nar/gkn188.
39. Gruber, A. R.; Bernhart, S. H.; Lorenz, R. *The ViennaRNA web services*. RNA bioinformatics: New York, NY, USA, **2015**; pp 307-326, https://doi.org/10.1007/978-1-4939-2291-8_19.
40. Bonnet, J.; Colotte, M.; Coudy, D.; Couallier, V.; Portier, J.; Morin, B.; Tuffet, S. Chain and conformation stability of solid-state DNA: implications for room temperature storage. *Nucleic acids research* **2010**, *38*, 1531-1546, https://doi.org/10.1093/nar/gkp1060.
41. Zuker, M. Mfold web server for nucleic acid folding and hybridization prediction. *Nucleic acids research* **2003**, *31*, 3406-3415, https://doi.org/10.1093/nar/gkg595.
42. Ghosh, S.; Takahashi, S.; Ohyama, T.; Endoh, T.; Tateishi-Karimata, H.; Sugimoto, N. Nearest-neighbor parameters for predicting DNA duplex stability in diverse molecular crowding conditions. *Proceedings of the National Academy of Sciences* **2020**, *117*, 14194-14201, https://doi.org/10.1073/pnas.1920886117.
43. Sugimoto, N.; Endoh, T.; Takahashi, S.; Tateishi-Karimata, H. Chemical biology of double helical and non-double helical nucleic acids: "to B or not to B, that is the question". *Bulletin of the Chemical Society of Japan* **2021**, *94*, 1970-1998, https://doi.org/10.1246/bcsj.20210131.
44. Land, H., Humble, M. S. *YASARA: a tool to obtain structural guidance in biocatalytic investigations*. *Protein Engineering: New York, NY, USA*, **2018**; 43-67, https://doi.org/10.1007/978-1-4939-7366-8_4.
45. Smith, M. D.; Rao, J. S.; Segelken, E.; Cruz, L. Force-field induced bias in the structure of Aβ21–30: A comparison of OPLS, AMBER, CHARMM, and GROMOS force fields. *Journal of Chemical Information and Modeling* **2015**, *55*, 2587-2595, https://doi.org/10.1021/acs.jcim.5b00308.
46. Mark, P.; Nilsson, L. Structure and dynamics of the TIP3P, SPC, and SPC/E water models at 298 K. *The Journal of Physical Chemistry A*. **2001**, *105*, 9954-9960, https://doi.org/10.1021/jp003020w.
47. Luty, B. A.; van Gunsteren, W. F. Calculating electrostatic interactions using the particle− particle particle− mesh method with nonperiodic long-range interactions. *The Journal of Physical Chemistry* **1996**, *100*, 2581-2587, https://doi.org/10.1021/jp9518623.
48. Petersen, H. G. Accuracy and efficiency of the particle mesh Ewald method. *The Journal of chemical physics* **1995**, *103*, 3668-3679, https://doi.org/10.1063/1.470043.
49. Friedman, R. A.; Honig, B. The electrostatic contribution to DNA base-stacking interactions. *Biopolymers: Original Research on Biomolecules* **1992**, *32*, 145-159, https://doi.org/10.1002/bip.360320205.
50. Knight, C. J.; Hub, J. S. WAXSiS: a web server for the calculation of SAXS/WAXS curves based on explicit-solvent molecular dynamics. *Nucleic acids research* **2015**, *43*, W225-W230, https://doi.org/10.1093/nar/gkv309.
51. Kusumaningrum, S., Budianto, E., Kosela, S., Sumaryono, W., & Juniarti, F. The molecular docking of 1, 4-naphthoquinone derivatives as inhibitors of Polo-like kinase 1 using Molegro Virtual Docker. Journal of Applied Pharmaceutical Science **2014**, 4(11), 047-053. https://doi.org/10.7324/JAPS.2014.4119
52. Jejurikar, B. L.; Rohane, S. H. Drug designing in discovery studio. *Asian Journal of Research in Chemistry* **2021**, *14*, 135-138, https://doi.org/10.5958/0974-4150.2021.00025.0.
53. Patel, N.; Dubins, D. N.; Pomès, R.; Chalikian, T. V. Size dependence of cavity volume: A molecular dynamics study. *Biophysical Chemistry* **2012**, *161*, 46-49, https://doi.org/10.1016/j.bpc.2011.10.001.
54. Xavier Senra, M. V.; Fonseca, A. L. New tyrosinases with putative action against contaminants of emerging concern. *Proteins: Structure, Function, and Bioinformatics* **2021**, *89*, 1180-1192, https://doi.org/10.1002/prot.26139.
55. Gautam, V.; Chong, W. L.; Chin, S. P.; Zain, S. M.; Rahman, N. A.; Vao-soongnern, V.; Lee, V. S. Loop dynamics behind the affinity of DARPins towards ERK2: Molecular dynamics simulations (MDs) and elastic network model (ENM). *Journal of Molecular Liquids* **2019**, *274*, 612-620, https://doi.org/10.1016/j.molliq.2018.10.157.
56. Madhavi, W. M.; Weerasinghe, S.; Momot, K. I. Reorientational dynamics of molecules in liquid methane: A molecular dynamics simulation study. *Journal of Molecular Liquids* **2021**, *324*, 114727, https://doi.org/10.1016/j.molliq.2020.114727.
57. Yonezawa, Y. Electrostatic properties of water models evaluated by a long-range potential based solely on the Wolf charge-neutral condition. *Chemical Physics Letters* **2013**, *556*, 308-314, https://doi.org/10.1016/j.cplett.2012.12.028.

58. Kräutler, V.; Van Gunsteren, W. F.; Hünenberger, P. H. A fast SHAKE algorithm to solve distance constraint equations for small molecules in molecular dynamics simulations. *Journal of computational chemistry* **2001**, *22*, 501-508, https://doi.org/10.1002/1096-987X(20010415)22:5%3C501::AID-JCC1021%3E3.0.CO;2-V.
59. Kasahara, K.; Ma, B.; Goto, K.; Dasgupta, B.; Higo, J.; Fukuda, I.; ... Nakamura, H. myPresto/omegagene: a GPU-accelerated molecular dynamics simulator tailored for enhanced conformational sampling methods with a non-Ewald electrostatic scheme. *Biophysics and physicobiology* **2016**, *13*, 209-216, https://doi.org/10.2142/biophysico.13.0_209.
60. Dupuis, N.; Holmstrom, E.; Nesbitt, D. Molecular-crowding effects on single-molecule RNA folding/unfolding thermodynamics and kinetics. *Proceedings of the National Academy of Sciences* **2014**, *111*, 8464-8469, https://doi.org/10.1073/pnas.1316039111.
61. Kalwarczyk, T.; Ziebacz, N.; Bielejewska, A.; Zaboklicka, E.; Koynov, K.; Szymanski, J.; Hołyst, R. Comparative analysis of viscosity of complex liquids and cytoplasm of mammalian cells at the nanoscale. *Nano letters* **2011**, *11*, 2157-2163, https://doi.org/10.1021/nl2008218.
62. Regan, K.; Dotterweich, R.; Ricketts, S.; Robertson-Anderson, R. M. Diffusion and conformational dynamics of single DNA molecules crowded by cytoskeletal proteins. *Journal of Undergraduate Reports in Physics* **2018**, *28*, 100005, https://doi.org/10.1063/1.5109559.
63. Garbett, N. C.; Mekmaysy, C. S.; Chaires, J. B. *Sedimentation velocity ultracentrifugation analysis for hydrodynamic characterization of G-quadruplex structures*. G-Quadruplex DNA: *Totowa, NJ, USA*, **2010**; 97-120, https://doi.org/10.1007/978-1-59745-363-9_7.
64. Phillips, R.; Kondev, J.; Theriot, J. Life in Crowded and Disordered Environments. *Physical Biology of the Cell*; Garland Science: *New York, USA*, **2009**; 1057, 1-29.
65. Schavemaker, P. E.; Boersma, A. J.; Poolman, B. How important is protein diffusion in prokaryotes?. *Frontiers in Molecular Biosciences* **2018**, *5*, 93, https://doi.org/10.3389/fmolb.2018.00093.
66. Malinowski, E. R.; Howery, D. G. *Factor analysis in chemistry*; Wiley: New York, NY, USA, 1980; 432, https://analyticalscience.wiley.com/do/10.1002/sepspec.9780471134794.
67. StatSoft, Inc. STATISTICA (data analysis software system); INC StatSoft: Tulsa, USA, 2007, 91-94.
68. Nitsche, A.; Ellerbrok, H.; Pauli, G. Detection of orthopoxvirus DNA by real-time PCR and identification of variola virus DNA by melting analysis. *Journal of clinical microbiology* **2004**, *42*, 1207-1213, https://doi.org/10.1128/JCM.42.3.1207-1213.2004 .
69. Baker, M. A.; Tuckwell, A. J.; Berengut, J. F.; Bath, J.; Benn, F.; Duff, A. P.; ... Lee, L. K. Dimensions and global twist of single-layer DNA origami measured by small-angle X-ray scattering. *ACS nano* **2018**, *12*, 5791-5799, https://doi.org/10.1021/acsnano.8b01669.
70. Gun'ko, V. M.; Meikle, S. T.; Kozynchenko, O. P.; Tennison, S. R.; Ehrburger-Dolle, F.; Morfin, I.; Mikhalovsky, S. V. Comparative characterization of carbon adsorbents and polymer precursors by small-angle X-ray scattering and nitrogen adsorption methods. *The Journal of Physical Chemistry C* **2011**, *115*, 10727-10735, https://doi.org/10.1021/jp201835r.
71. González-Paz, L.; Alvarado, M. J.; Hurtado-León, M. L.; Lossada, C.; Vera-Villalobos, J.; Loroño, M., Paz, J. L.; Jeffreys, L. N.; Torres, F. J.; Alvarado, Y. J. Comparative study of SARS-CoV-2 infection in different cell types: Biophysical-computational approach to the role of potential receptors. *Computers in biology and medicine* **2022**, *142*, 105245, https://doi.org/10.1016/j.compbiomed.2022.105245.
72. Di Michele, L.; Mognetti, B. M.; Yanagishima, T.; Varilly, P.; Ruff, Z.; Frenkel, D.; Eiser, E. Effect of inert tails on the thermodynamics of DNA hybridization. *Journal of the American Chemical Society* **2014**, *136*, 6538-6541, https://doi.org/10.1021/ja500027v.
73. Allawi, H. T.; SantaLucia, J. Nearest-Neighbor Thermodynamics of Internal A. C Mismatches in DNA: Sequence Dependence and pH Effects. *Biochemistry* **1998**, *37*, 9435-9444. https://doi.org/10.1021/bi9803729.
74. Parra, A. E.; Antequera, L.; Lossada, C. A.; Fernández-Materán, F. V.; Parra, M. M.; Centanaro, P.; González-Paz, L. A. Comparative Analysis of CRISPR-Cas Systems in Vibrio and Photobacterium Genomes of High Influence in Aquaculture Production. *Biointerface Research in Applied Chemistry* **2020,** *11*, 9513-9529, https://doi.org/10.33263/BRIAC112.95139529.
75. Keckler, M. S.; Salzer, J. S.; Patel, N.; Townsend, M. B.; Nakazawa, Y. J.; Doty, J. B.; Damon, I. K. IMVAMUNE® and ACAM2000® provide different protection against disease when administered postexposure in an intranasal monkeypox challenge prairie dog model. *Vaccines* **2020**, *8*, 396, https://doi.org/10.3390/vaccines8030396.
76. Hutson, C. L.; Kondas, A. V.; Mauldin, M. R.; Doty, J. B.; Grossi, I. M.; Morgan, C. N.; Olson, V. A. Pharmacokinetics and efficacy of a potential smallpox therapeutic, brincidofovir, in a lethal monkeypox virus animal model. *MSphere* **2021**, *6*, e00927-20, https://doi.org/10.1128/mSphere.00927-20.
77. Cao, S.; Realegeno, S.; Pant, A.; Satheshkumar, P. S.; Yang, Z. Suppression of poxvirus replication by resveratrol. *Frontiers in Microbiology* **2017**, *8*, 2196, https://doi.org/10.3389/fmicb.2017.02196.
78. Kulesh, D. A.; Loveless, B. M.; Norwood, D.; Garrison, J.; Whitehouse, C. A.; Hartmann, C.; Ludwig, G. V. Monkeypox virus detection in rodents using real-time 3′-minor groove binder TaqMan® assays on the Roche LightCycler. *Laboratory investigation* **2004**, *84*, 1200-1208, https://doi.org/10.1038/labinvest.3700143.

79. Sweeney, P.; Galliford, A.; Kumar, A.; Raju, D.; Krishna, N. B.; Sutherland, E.; da Silva, R. G. Structure, dynamics, and molecular inhibition of the Staphylococcus aureus m1A22-tRNA methyltransferase TrmK. *Journal of Biological Chemistry* **2022**, *298*, 102040, https://doi.org/10.1016/j.jbc.2022.102040.
80. Antunes, D.; Santos, L. H.; Caffarena, E. R.; Guimarães, A. C. R. Bacterial 2′-Deoxyguanosine Riboswitch Classes as Potential Targets for Antibiotics: A Structure and Dynamics Study. *International Journal of Molecular Sciences* **2022**, *23*, 1925, https://doi.org/10.3390/ijms23041925.
81. Roy, S.; Ali, A.; Bhattacharya, S. Theoretical insight into the library screening approach for binding of intermolecular G-quadruplex RNA and small molecules through docking and molecular dynamics simulation studies. *The Journal of Physical Chemistry B.* **2021**, *125*, 5489-5501, https://doi.org/10.1021/acs.jpcb.0c10991 .
82. Ishida, H.; Kono, H. Torsional stress can regulate the unwrapping of two outer half superhelical turns of nucleosomal DNA. *Proceedings of the National Academy of Sciences* **2021**, *118*, e2020452118, https://doi.org/10.1073/pnas.2020452118.
83. Pérez-Juárez, J.; Tapia-Vieyra, J. V.; Gutiérrez-Magdaleno, G.; Sánchez-Puig, N. Altered Conformational Landscape upon Sensing Guanine Nucleotides in a Disease Mutant of Elongation Factor-like 1 (EFL1) GTPase. *Biomolecules* **2022**, *12*, 1141, https://doi.org/10.3390/biom12081141.
84. Shahabadi, N.; Shiri, F.; Khodarahmi, R. A Cu (I) complex groove binder with a high affinity towards DNA denaturation. *Journal of Molecular Liquids* **2022**, *345*, 117904, https://doi.org/10.1016/j.molliq.2021.117904.
85. Tomek, K. J.; Volkel, K.; Indermaur, E. W.; Tuck, J. M.; Keung, A. J. Promiscuous molecules for smarter file operations in DNA-based data storage. *Nature communications* **2021**, *12*, 1-10, https://doi.org/10.1038/s41467-021-23669-w.
86. Jain, A.; Rophina, M.; Mahajan, S.; Krishnan, B. B.; Sharma, M.; Mandal, S.; Scaria, V. Analysis of the potential impact of genomic variants in global SARS-CoV-2 genomes on molecular diagnostic assays. *International Journal of Infectious Diseases* **2021**, *102*, 460-462, https://doi.org/10.1016/j.ijid.2020.10.086.
87. Harshitha, R.; Arunraj, D. R. Real-time quantitative PCR: A tool for absolute and relative quantification. *Biochemistry and Molecular Biology Education* **2021**, *49*, 800-812, https://doi.org/10.1002/bmb.21552.
88. Rejali, N. A.; Ye, F. D.; Zuiter, A. M.; Keller, C. C.; Wittwer, C. T. Nearest-neighbour transition-state analysis for nucleic acid kinetics. *Nucleic Acids Research* **2021**, *49*, 4574-4585, https://doi.org/10.1093/nar/gkab205.
89. Miranda, P.; Weber, G. Thermodynamic evaluation of the impact of DNA mismatches in PCR-type SARS-CoV-2 primers and probes. *Molecular and cellular probes* **2021**, *56*, 101707, https://doi.org/10.1016/j.mcp.2021.101707.
90. Miranda, P.; Barbosa, V. B.; Weber, G. Mesoscopic Evaluation of DNA Mismatches in PCR Primer-Target Hybridisation to Detect SARS-CoV-2 Variants of Concern. *In Brazilian Symposium on Bioinformatics* (BSB 2021)**2021**, 145-150, https://link.springer.com/chapter/10.1007/978-3-030-91814-9_15.

Supplementary materials

Table S1. Proposed primers for the specific detection of MpxV.

Primer ID	Sequence (5'-->3')
P1 - OPG191	TG TG GG TA CC GG AC TA CG AT
P1 - OPG117	TC GG TG AC CT GT TT GT CG AG
P1 - OPG118	TT GT TG TT CG CC TT GG TA GC
P1 - OPG032	CT GC CA AG AT AG CT TC AG AG T
P1 - OPG035	AG CA AT GG AC CG TC GG AT AG
P1 - OPG047	GG AA CC AA CG CT CA AC AG AT G
P1 - OPG190	TG CG TA CT AC CT GC TG TT GT
P1 - OPG200	TG CG CT GG AC AA CT GT AT GA
P2 - OPG191	CA CC TC CA GT GA TC GT AC CA A
P2 - OPG117	TC AG CA GC CT CT CT AC CA GA
P2 - OPG118	TG AG TA CA TT CA CT CC GC GT
P2 - OPG032	CC CA AT GC GG GC GA TG TA
P2 - OPG035	GG AG AA AT GA CG GC GA TC CA
P2 - OPG047	CT CC GA TG AA TA GC CC CA GA
P2 - OPG190	CG CA TT AG GA CA CG TG AC AG
P2 - OPG200	CC TC CC CA GT AA GT AG CA GC

Query	1	TGTGGGTACCGGACTACGAT	20
OP022171.1	166393	....	166412
OP022170.1	166405	....	166424
OP019277.1	166399	....	166418
OP019276.1	166399	....	166418
OP019275.1	166402	....	166421
OP018607.1	166402	....	166421
OP018606.1	166401	....	166420
OP018605.1	166402	....	166421
OP018604.1	166402	....	166421
OP018603.1	166402	....	166421
OP018602.1	166401	....	166420
OP018601.1	166402	....	166421
OP018600.1	166402	....	166421
OP018599.1	166401	....	166420
OP018598.1	166401	....	166420
OP018597.1	166401	....	166420
OP018596.1	166401	....	166420
OP018595.1	166402	....	166421
OP018594.1	166402	....	166421
OP018593.1	166402	....	166421
OP018592.1	166401	....	166420
OP018591.1	166401	....	166420
OP018590.1	166402	....	166421
OP018589.1	166402	....	166421
OP018588.1	166402	....	166421
OP013017.1	166395	....	166414
OP013016.1	166388	....	166407
OP013015.1	166395	....	166414
OP013014.1	166395	....	166414
OP013013.1	166395	....	166414
OP013012.1	166395	....	166414
OP013011.1	166394	....	166413
OP013010.1	166395	....	166414
OP013009.1	166395	....	166414
OP013008.1	166395	....	166414
OP013007.1	166396	....	166415
OP013006.1	166398	....	166417
OP013005.1	166395	....	166414
OP013004.1	166395	....	166414
OP013003.1	166395	....	166414
OP013002.1	166405	....	166424
OP013001.1	166384	....	166403
OP012849.1	166403	....	166422
ON983168.1	165088	....	165107
ON983167.1	166395	....	166414
ON983166.1	166392	....	166411
ON983165.1	166391	....	166410
ON983164.1	166395	....	166414
ON983163.1	166395	....	166414
ON983162.1	166395	....	166414

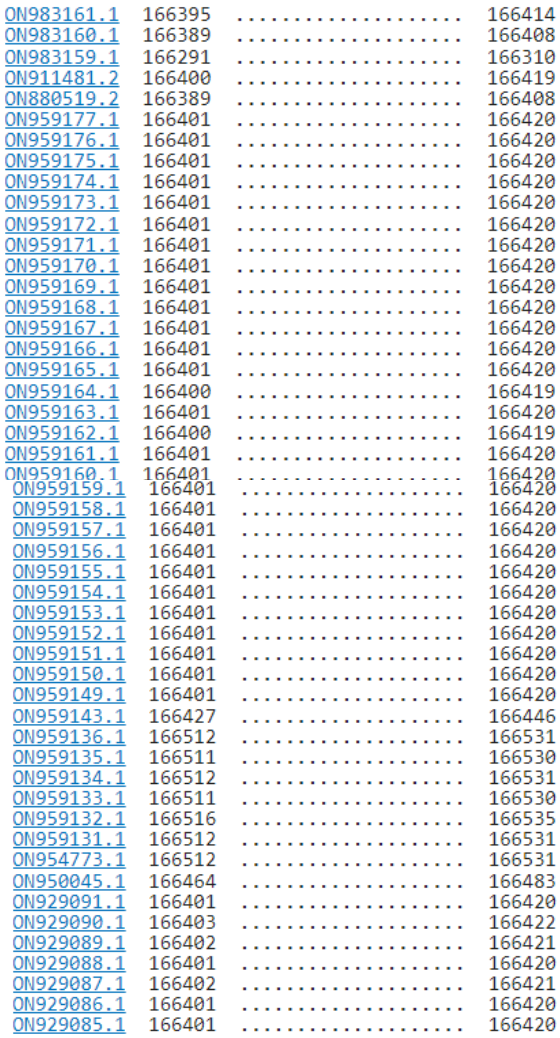

Figure S1. Associated "join region" annotation. For illustrative purposes, the Associated "binding region" annotation for Primer-ID = P1 - OPG191 is shown. The rest of the regions can be predicted using the BLAST tool.

Table S2. Genomic sequences used for the prediction of primers directed to genes associated with *Monkeypox virus* (MpxV).

Accession*	Genome(s)	Date
OX009124.1	*Monkeypox virus* isolate lesión	9-jun-22
ON880549.1	*Monkeypox virus* isolate MpxV/human/CAN/UN-NML-3450/2022	
ON880548.1	*Monkeypox virus* isolate MpxV/human/CAN/UN-NML-3448/2022	
ON880547.1	*Monkeypox virus* isolate MpxV/human/CAN/UN-NML-3441/2022	
ON880546.1	*Monkeypox virus* isolate MpxV/human/CAN/UN-NML-3368/2022	
ON880545.1	*Monkeypox virus* isolate MpxV/human/CAN/UN-NML-3366/2022	
ON880544.1	*Monkeypox virus* isolate MpxV/human/CAN/UN-NML-3363/2022	
ON880543.1	*Monkeypox virus* isolate MpxV/human/CAN/UN-NML-3357/2022	
ON880542.1	*Monkeypox virus* isolate MpxV/human/CAN/UN-NML-3348/2022	
ON880541.1	*Monkeypox virus* isolate MpxV/human/CAN/UN-NML-3344/2022	
ON880540.1	*Monkeypox virus* isolate MpxV/human/CAN/UN-NML-3342/2022	
ON880539.1	*Monkeypox virus* isolate MpxV/human/CAN/UN-NML-3339/2022	30-jun-22
ON880538.1	*Monkeypox virus* isolate MpxV/human/CAN/UN-NML-3336/2022	
ON880537.1	*Monkeypox virus* isolate MpxV/human/CAN/UN-NML-3273/2022	
ON880536.1	*Monkeypox virus* isolate MpxV/human/CAN/UN-NML-3272/2022	
ON880535.1	*Monkeypox virus* isolate MpxV/human/CAN/UN-NML-3269/2022	
ON880534.1	*Monkeypox virus* isolate MpxV/human/CAN/UN-NML-3262/2022	
ON880533.1	*Monkeypox virus* isolate MpxV/human/CAN/UN-NML-3257/2022	
ON880532.1	*Monkeypox virus* isolate MpxV/human/CAN/UN-NML-3253/2022	
ON880531.1	*Monkeypox virus* isolate MpxV/human/CAN/UN-NML-3165/2022	
ON880530.1	*Monkeypox virus* isolate MpxV/human/CAN/UN-NML-3162/2022	
ON880529.1	*Monkeypox virus* isolate MpxV/human/CAN/UN-NML-3153/2022	

Accession*	Genome(s)	Date
ON880528.1	*Monkeypox virus* isolate MpxV/human/CAN/UN-NML-3147/2022	
ON880527.1	*Monkeypox virus* isolate MpxV/human/CAN/UN-NML-3141/2022	
ON880526.1	*Monkeypox virus* isolate MpxV/human/CAN/UN-NML-3100/2022	
ON880525.1	*Monkeypox virus* isolate MpxV/human/CAN/UN-NML-3086/2022	
ON880524.1	*Monkeypox virus* isolate MpxV/human/CAN/UN-NML-3080/2022	
ON880523.1	*Monkeypox virus* isolate MpxV/human/CAN/UN-NML-2898/2022	
ON880522.1	*Monkeypox virus* isolate MpxV/human/CAN/UN-NML-2870/2022	
ON880521.1	*Monkeypox virus* isolate MpxV/human/CAN/UN-NML-2858/2022	
ON880520.1	*Monkeypox virus* isolate MpxV/human/CAN/UN-NML-2857/2022	
ON880519.1	*Monkeypox virus* isolate MpxV/human/CAN/UN-NML-2833/2022	
ON880518.1	*Monkeypox virus* isolate MpxV/human/CAN/UN-NML-3486/2022	
ON880517.1	*Monkeypox virus* isolate MpxV/human/CAN/UN-NML-3476/2022	
ON880516.1	*Monkeypox virus* isolate MpxV/human/CAN/UN-NML-3472/2022	
ON880515.1	*Monkeypox virus* isolate MpxV/human/CAN/UN-NML-3467/2022	
ON880514.1	*Monkeypox virus* isolate MpxV/human/CAN/UN-NML-3412/2022	
ON880513.1	*Monkeypox virus* isolate MpxV/human/CAN/UN-NML-3407/2022	
ON880512.1	*Monkeypox virus* isolate MpxV/human/CAN/UN-NML-3292/2022	
ON880511.1	*Monkeypox virus* isolate MpxV/human/CAN/UN-NML-3214/2022	
ON880510.1	*Monkeypox virus* isolate MpxV/human/CAN/UN-NML-3193/2022	
ON880509.1	*Monkeypox virus* isolate MpxV/human/CAN/UN-NML-3137/2022	
ON880508.1	*Monkeypox virus* isolate MpxV/human/CAN/UN-NML-3127/2022	
ON880507.1	*Monkeypox virus* isolate MpxV/human/CAN/UN-NML-3071/2022	
ON880506.1	*Monkeypox virus* isolate MpxV/human/CAN/UN-NML-2959/2022	
ON880505.1	*Monkeypox virus* isolate MpxV/human/CAN/UN-NML-2906/2022	30-jun-22
ON880422.1	*Monkeypox virus* isolate MPX/UZ_REGA_6/Belgium/2022	
ON880421.1	*Monkeypox virus* isolate MPX/UZ_REGA_5/Belgium/2022	
ON880420.1	*Monkeypox virus* isolate MPX/UZ_REGA_4/Belgium/2022	
ON880419.1	*Monkeypox virus* isolate MPX/UZ_REGA_3/Belgium/2022	
ON880413.1	*Monkeypox virus* isolate MPX/BR0002/2022	
ON872184.1	*Monkeypox virus* strain WA-2022	29-jun-22
ON853682.1	*Monkeypox virus* isolate MPXV/Germany/2022/RKI101	
ON853681.1	*Monkeypox virus* isolate MPXV/Germany/2022/RKI092	
ON853680.1	*Monkeypox virus* isolate MPXV/Germany/2022/RKI097	
ON853679.1	*Monkeypox virus* isolate MPXV/Germany/2022/RKI077	
ON853678.1	*Monkeypox virus* isolate MPXV/Germany/2022/RKI100	
ON853677.1	*Monkeypox virus* isolate MPXV/Germany/2022/RKI099	
ON853676.1	*Monkeypox virus* isolate MPXV/Germany/2022/RKI098	
ON853675.1	*Monkeypox virus* isolate MPXV/Germany/2022/RKI096	
ON853674.1	*Monkeypox virus* isolate MPXV/Germany/2022/RKI095	
ON853673.1	*Monkeypox virus* isolate MPXV/Germany/2022/RKI094	
ON853672.1	*Monkeypox virus* isolate MPXV/Germany/2022/RKI093	
ON853671.1	*Monkeypox virus* isolate MPXV/Germany/2022/RKI091	
ON853670.1	*Monkeypox virus* isolate MPXV/Germany/2022/RKI090	
ON853669.1	*Monkeypox virus* isolate MPXV/Germany/2022/RKI089	
ON853668.1	*Monkeypox virus* isolate MPXV/Germany/2022/RKI086	
ON853667.1	*Monkeypox virus* isolate MPXV/Germany/2022/RKI085	27-jun-22
ON853666.1	*Monkeypox virus* isolate MPXV/Germany/2022/RKI084	
ON853664.1	*Monkeypox virus* isolate MPXV/Germany/2022/RKI082	
ON853663.1	*Monkeypox virus* isolate MPXV/Germany/2022/RKI081	
ON853662.1	*Monkeypox virus* isolate MPXV/Germany/2022/RKI080	
ON853661.1	*Monkeypox virus* isolate MPXV/Germany/2022/RKI079	
ON853660.1	*Monkeypox virus* isolate MPXV/Germany/2022/RKI078	
ON853659.1	*Monkeypox virus* isolate MPXV/Germany/2022/RKI075	
ON853658.1	*Monkeypox virus* isolate MPXV/Germany/2022/RKI072	
ON853657.1	*Monkeypox virus* isolate MPXV/Germany/2022/RKI071	
ON853656.1	*Monkeypox virus* isolate MPXV/Germany/2022/RKI070	
ON853655.1	*Monkeypox virus* isolate MPXV/Germany/2022/RKI088	
ON853654.1	*Monkeypox virus* isolate MPXV/Germany/2022/RKI087	
ON853653.1	*Monkeypox virus* isolate MPXV/Germany/2022/RKI076	
ON853652.1	*Monkeypox virus* isolate MPXV/Germany/2022/RKI074	
ON853651.1	*Monkeypox virus* isolate MPXV/Germany/2022/RKI073	
ON853650.1	*Monkeypox virus* isolate MPXV/Germany/2022/RKI069	

Accession*	Genome(s)	Date
ON853649.1	*Monkeypox virus* isolate MPXV/Germany/2022/RKI068	
ON843182.1	*Monkeypox virus* isolate Monkeypox/PT0044/2022	
ON843181.1	*Monkeypox virus* isolate Monkeypox/PT0045/2022	
ON843180.1	*Monkeypox virus* isolate Monkeypox/PT0042/2022	
ON843179.1	*Monkeypox virus* isolate Monkeypox/PT0039/2022	
ON843178.1	*Monkeypox virus* isolate Monkeypox/PT0040/2022	
ON843177.1	*Monkeypox virus* isolate Monkeypox/PT0047/2022	
ON843176.1	*Monkeypox virus* isolate Monkeypox/PT0041/2022	
ON843175.1	*Monkeypox virus* isolate Monkeypox/PT0043/2022	24-jun-22
ON843174.1	*Monkeypox virus* isolate Monkeypox/PT0046/2022	
ON843173.1	*Monkeypox virus* isolate Monkeypox/PT0029/2022	
ON843172.1	*Monkeypox virus* isolate Monkeypox/PT0035/2022	
ON843171.1	*Monkeypox virus* isolate Monkeypox/PT0030/2022	
ON843169.1	*Monkeypox virus* isolate Monkeypox/PT0034/2022	
ON843168.1	*Monkeypox virus* isolate Monkeypox/PT0032/2022	
ON843167.1	*Monkeypox virus* isolate Monkeypox/PT0036/2022	

*NCBI/GenBank (https://www.ncbi.nlm.nih.gov/).

Table S3. Thermodynamic stability of the primers.

	DNAfold				MFEp		FastPCR				
	kcal/mol		cal/(K·mol)	°C	kcal/mol	°C	kcal/mol		cal/(K·mol)	°C	°C
Primer ID	ΔG_DNAf	ΔH_DNAf	ΔS_DNAf	Tm_DNAf	ΔG_MFEp	Tm_MFEp	ΔG_Fast	ΔH_Fast	ΔS_Fast	Tm_Fast1	Tm_Fast2
P1 - OPG191	-1.3	-27.3	-83.7	52.6	-22.0	60.6	-25.7	-153.4	-431.9	63.2	64.4
P1 - OPG117	-0.2	-36.2	-116.2	38.3	-22.3	60.5	-25.9	-158.1	-446.1	62.8	64.4
P1 - OPG118	0.6	-4.5	-16.5	-1.0	-21.8	59.6	-25.4	-157.1	-444.4	61.6	62.3
P1 - OPG032	-0.3	-35.6	-113.8	39.4	-21.4	58.0	-25.1	-160.7	-457.9	60.1	62.6
P1 - OPG035	-0.2	-21.9	-69.9	40.1	-22.0	60.1	-25.7	-156.1	-440.6	62.6	64.4
P1 - OPG047	0.4	-14.5	-47.9	29.0	-22.8	60.3	-26.6	-166.5	-471.9	62.3	64.6
P1 - OPG190	-0.4	-23.7	-75.1	42.0	-21.8	59.8	-25.4	-155.3	-438.6	62.0	62.3
P1 - OPG200	-0.03	-23.3	-75.0	37.3	-22.0	60.2	-25.6	-155.6	-439.0	62.3	62.3
P2 - OPG191	-1.3	-31.3	-96.6	50.5	-22.4	60.0	-26.2	-162.3	-459.8	62.3	64.6
P2 - OPG117	0.3	-17.1	-56.1	31.3	-21.8	60.2	-25.3	-151.7	-427.3	63.0	64.4
P2 - OPG118	-1.3	-44.3	-138.5	46.6	-21.8	59.6	-25.4	-156.0	-441.0	61.7	62.3
P2 - OPG032	-1.4	-31.6	-97.3	51.4	-21.3	60.7	-24.6	-142.0	-396.6	63.6	64.0

	DNAfold				MFEp		FastPCR				
	kcal/mol		cal/(K·mol)	°C	kcal/mol	°C	kcal/mol		cal/(K·mol)	°C	°C
Primer ID	ΔG_DNAf	ΔH_DNAf	ΔS_DNAf	Tm_DNAf	ΔG_MFEp	Tm_MFEp	ΔG_Fast	ΔH_Fast	ΔS_Fast	Tm_Fast1	Tm_Fast2
P2 - OPG035	-0.2	-21.8	-69.6	39.8	-22.3	60.7	-26.0	-157.0	-442.5	63.1	64.4
P2 - OPG047	1.3	-6.7	-25.7	-13.3	-21.4	59.2	-25.0	-152.7	-431.7	61.9	64.4
P2 - OPG190	0.7	-11.4	-39.0	18.8	-22.1	59.5	-25.6	-160.7	-455.3	61.6	64.4
P2 - OPG200	0.8	-20.7	-69.3	25.3	-21.9	60.1	-25.5	-154.7	-436.5	62.9	66.4

ΔG_DNAf, minimum free energy for formation predicted with DNAfold; ΔH_DNAf, predicted enthalpy with DNAfold; ΔS_DNAf, predicted entropy with DNAfold; Tm_DNAf, predicted fusion temperature with DNAfold; ΔG_MFEp, minimum free energy for formation predicted with MFE; Tm_MFEp, melting temperature predicted with MFE; ΔG_Fast, minimum free energy for formation predicted with FastPCR; ΔH_Fast, enthalpy predicted with FastPCR; ΔS_Fast, predicted entropy with FastPCR; Tm_Fast1, melting temperature # 1 predicted with FastPCR; Tm_Fast2, fusion temperature # 2 predicted with FastPCR.

Table S4. Dynamic stability of the primers and their conformational fluctuations in solution.

Primer ID	Rg (Å)	RMSD (Å)	ε (%)	subopt	*D*1	t1	*D*2	t2	*D*3	t3
P1 - OPG191	20.0	1.8	83	69	2.49	2.4E-04	4.57	1.3E-04	1.09	5.5E-04
P1 - OPG117	20.2	2.4	77	143	2.47	2.4E-04	4.53	1.3E-04	1.08	5.6E-04
P1 - OPG118	20.2	2.4	71	116	2.47	2.4E-04	4.53	1.3E-04	1.08	5.6E-04
P1 - OPG032	21.0	2.5	90	66	2.38	2.5E-04	4.37	1.4E-04	1.04	5.8E-04
P1 - OPG035	20.2	2.6	87	18	2.48	2.4E-04	4.54	1.3E-04	1.08	5.6E-04
P1 - OPG047	20.6	3.0	85	14	2.43	2.5E-04	4.45	1.3E-04	1.06	5.7E-04
P1 - OPG190	20.0	2.3	71	91	2.49	2.4E-04	4.57	1.3E-04	1.09	5.5E-04
P1 - OPG200	20.0	3.1	87	42	2.49	2.4E-04	4.57	1.3E-04	1.09	5.5E-04
P2 - OPG191	20.9	2.4	87	12	2.39	2.5E-04	4.39	1.4E-04	1.05	5.7E-04
P2 - OPG117	20.1	2.2	68	27	2.48	2.4E-04	4.55	1.3E-04	1.09	5.5E-04
P2 - OPG118	20.2	2.5	95	35	2.47	2.4E-04	4.52	1.3E-04	1.08	5.6E-04
P2 - OPG032	18.3	2.1	66	22	2.72	2.2E-04	5.00	1.2E-04	1.20	5.0E-04
P2 - OPG035	20.2	2.5	84	19	2.47	2.4E-04	4.54	1.3E-04	1.08	5.6E-04
P2 - OPG047	20.1	2.4	82	7	2.48	2.4E-04	4.56	1.3E-04	1.09	5.5E-04
P2 - OPG190	20.1	1.5	79	12	2.49	2.4E-04	4.56	1.3E-04	1.09	5.5E-04
P2 - OPG200	20.5	2.5	58	10	2.43	2.5E-04	4.46	1.3E-04	1.07	5.6E-04

Rg, radius of gyration; RMSD, root mean square deviation; **ε**, efficiency of the PCR reaction predicted with FastPCR; Subopt, # of minimum energy substructures predicted with DNAfold; *D*1, diffusion coefficient predicted with model 1 HeLa (with a cytoplasmic viscosity of ~4.4×10^{-2} Pa/s) [63]; t1, diffusion rate predicted with model 1; *D*2, diffusion coefficient predicted with model 2 (Normal Swiss 3T3 cells (with a viscosity of ~2.4×10^{-2} Pa/s) [63,64]; t2, diffusion rate predicted with model 2; *D*3, diffusion coefficient predicted with model 2 (viscosity of the water calculated with a viscosity of ~ 0.001 Pa/s) [65]); t3, diffusion rate predicted with model 3.

P1 - OPG191 = 37 ˚C
5'-TGTGGGTACCGGACTACGAT-3'

ΔG = -1.31

Structural element	δG	Information
External loop	-1.44	11 ss bases & 1 closing helices.
Stack	-2.17	External closing pair is C^{10}-G^{18}
Helix	-2.17	2 base pairs.
Hairpin loop	2.30	Closing pair is G^{11}-C^{17}

P2 - OPG191 = 37 ˚C
5'-CACCTCCAGTGATCGTACCAA-3'

ΔG = -1.31

Structural element	δG	Information
External loop	-0.92	10 ss bases & 1 closing helices.
Stack	-1.45	External closing pair is C^{1}-G^{11}
Stack	-1.44	External closing pair is A^{2}-T^{10}
Helix	-2.89	3 base pairs.
Hairpin loop	2.50	Closing pair is C^{3}-G^{9}

P1 - OPG191 = 95 ˚C
5'-TGTGGGTACCGGACTACGAT-3'

ΔG = 1.02

Structural element	δG	Information
External loop	-0.65	11 ss bases & 1 closing helices.
Stack	0.21	External closing pair is T^{3}-G^{11}
Stack	-0.69	External closing pair is G^{4}-C^{10}
Helix	-0.48	3 base pairs.
Hairpin loop	2.15	Closing pair is G^{5}-C^{9}

P2 - OPG191 = 95 ˚C
5'-CACCTCCAGTGATCGTACCAA-3'

ΔG = 2.03

Structural element	δG	Information
External loop	-1.25	12 ss bases & 1 closing helices.
Stack	-0.14	External closing pair is A^{2}-T^{10}
Helix	-0.14	2 base pairs.
Hairpin loop	3.42	Closing pair is C^{3}-G^{9}

Figure S2. Thermodynamic stability of OPG191 primers at 95 ˚C. For illustrative purposes, and by examining the thermodynamic stability of the OPG191 primers at 95 ˚C, as is a common condition in these reactions [6], the stability of the biomolecule, which does not undergo conformational changes at this temperature was confirmed, such as the formation of thermodynamically favorable hairpin-loops.

Table S5. Factor loadings (varimax normalized rotation) for variables of the 8 forward and reverse primers.

Variables	Factor 1	Factor 2	Factor 3	Factor 4	Factor 5
ΔG_DNAf	-0.25	**0.89**	0.09	0.12	0.04
ΔH_DNAf	0.02	**0.97**	-0.08	0.03	0.07
ΔS_DNAf	0.04	**0.96**	-0.10	0.02	0.07
Tm_DNAf	0.10	**-0.90**	-0.28	-0.03	0.02
ΔG_MFEp	0.44	0.01	**0.84**	0.26	0.00
Tm_MFEp	0.45	-0.12	**-0.86**	0.10	0.02
ΔG_Fast	0.58	0.01	**0.75**	0.29	-0.03
ΔH_Fast	**0.84**	-0.11	0.21	0.38	0.04
ΔS_Fast	**0.86**	-0.11	0.15	0.38	0.04
Tm_Fast1	0.53	-0.11	**-0.71**	0.35	0.16
Tm_Fast2	-0.12	0.14	-0.48	0.59	0.54
Rg (Å)	**-0.99**	0.03	0.03	-0.09	0.03
RMSD (Å)	-0.22	0.01	-0.17	-0.56	0.00
e (%)	-0.35	-0.35	0.13	**-0.72**	0.17
Subopt	-0.07	-0.10	0.03	0.07	**-0.97**
D1	**0.99**	-0.05	-0.03	0.07	0.00
t1	**-0.99**	0.03	0.04	-0.07	0.01
D2	**0.99**	-0.05	-0.02	0.08	0.00
t2	**-0.99**	0.03	0.03	-0.08	0.01
D3	**0.98**	-0.05	-0.01	0.13	0.03
t3	**-0.99**	0.03	0.02	-0.13	-0.02
Expl.Var	9.54	3.66	2.97	1.84	1.31
Prp.Totl	0.45	0.17	0.14	0.09	0.06

ΔG_DNAf, minimum free energy for formation predicted with DNAfold; ΔH_DNAf, predicted enthalpy with DNAfold; ΔS_DNAf, predicted entropy with DNAfold; Tm_DNAf, predicted fusion temperature with DNAfold; ΔG_MFEp, minimum free energy for formation predicted with MFE; Tm_MFEp, melting temperature predicted with MFE; ΔG_Fast, minimum free energy for formation predicted with FastPCR; ΔH_Fast, enthalpy predicted with FastPCR; ΔS_Fast, predicted entropy with FastPCR; Tm_Fast1, melting temperature #1 predicted with FastPCR; Tm_Fast2, fusion temperature #2 predicted with FastPCR; Rg, radius of gyration; RMSD, root mean square deviation; **ε**, efficiency of the PCR reaction predicted with FastPCR; Subopt, # of minimum energy substructures predicted with DNAfold; *D*1, diffusion coefficient predicted with model 1; t1, diffusion rate predicted with model 1; *D*2, diffusion coefficient predicted with model 2; t2, diffusion rate predicted with model 2; *D*3, diffusion coefficient predicted with model 2; t3, diffusion rate predicted with model 3.

All the parameters D1, t1, D2, t2, D3, t3, represent fluctuation components in solution, and are heavily loaded on factor 1 (F1). Most of the parameters that are predicted with FastPCR (eg, ΔH_Fast, ΔS_Fast, etc) and the Rg, are also heavily loaded (loadings > 0.70) on this factor. Thus, FastPCR and the other "F1 parameters" generate extensive redundancy and overlap between them. The second factor (F2) is almost exclusively a DNA fold dimension. This result showed that ΔG_DNAf, ΔH_DNAf, ΔS_DNAf and Tm_DNAf have a strong relationship. The third factor (F3) appears to be the most significant for MEFp functions such as ΔG_MFEp, Tm_MFEp, and for Tm predicted with FastPCR. Finally, F4 and F5 show high loadings for ε (PCR reaction efficiency) with FastPCR, RMSD and subopt. The indices with high loads on the same factor are interrelated, while there is no correlation between variables that have loads other than zero, only on different factors. Consequently, DNAfold metrics are orthogonal to most FastPCR parameters.

Table S4. Thermodynamic stability of the published primers.

Primer ID	Sequence (5'-->3')	DNAfold				Ref.
		kcal/mol		cal/(K·mol)	°C	
		ΔG_DNAf	ΔH_DNAf	ΔS_DNAf	Tm_DNAf	
P1 - OPG032	TGTCTACCTGGATACAGAAAGCAA	-3.3	-36.4	-106.8	67.6	12
P1 - OPG035	TTATTTTTCACCATATAGATCAATCATTAGATCAT	-1.6	-56.8	-178	45.8	79
P1 - OPG047	CTCATTGATTTTTCGCGGGAT	0.6	-8.4	-28.9	16.9	80
P1 - OPG190	ATTGGTCATTATTTTTGTCACAGGAACA	0.7	-25.2	-83.5	28.3	6
P1 - OPG191	ACGTGTTAAACAATGGGTGATG	-1.0	-22.5	-69.2	69.2	11
P2 - OPG032	GGCATCTCCGTTTAATACATTGAT	0.4	-11.7	-39	26.7	12
P2 - OPG035	ATGAGGACTCTACTTATTAGATATATTCTTTGGAG	-0.6	-15.8	-48.9	49.8	79
P2 - OPG047	GACGATACTCCTCCTCGTTGGT	-1.8	-19.6	-57.4	67.7	80
P2 - OPG190	AATGGCGTTGACAATTATGGGTG	-0.1	-14.6	-46.9	38.0	6
P2 - OPG191	AACATTTCCATGAATCGTAGTCC	-0.5	-16.4	-51.1	47.3	11

ΔG_DNAf, minimum free energy for formation predicted with DNAfold; ΔH_DNAf, predicted enthalpy with DNAfold; ΔS_DNAf, predicted entropy with DNAfold; Tm_DNAf, predicted fusion temperature with DNAfold.